AN ABSTRACT OF THE DISSERTATION OF

Phylicia Cicilio for the degree of Doctor of Philosophy in Electrical and Computer Engineering presented on March 4, 2020.

Title: Power System Planning for Sustainable, Reliable, and Accessible Electricity: Models, Methods, and Metrics

Abstract approved: _____

Dr. Eduardo Cotilla-Sanchez

Generation resources are shifting from centralized, high inertial, fossil fuel based to decentralized, no inertia, and variable renewable resources. The evolution of generation resources in electrical grids requires the transformation of the electrical grid infrastructure, and operation and planning procedures and standards. This dissertation takes four investigations into how to advance power system planning procedures and methods to integrate these resources into electrical grids ranging from minigrids to transmission systems. The first work addresses increasing energy access through development of sustainable off-grid minigrids through the introduction of an open-source planning tool which optimizes resource and equipment size and creates a distribution network placement map factoring in cost and reliability. The second work investigates the accuracy of measurement-based dynamic load modeling techniques used in transmission planning, highlighting the need for improvements of these commonly used methods due to a lack of correlation between model accuracy and output response error. The next work assesses the impact of dynamic loads and distributed energy resources (DERs), such as solar and wind, on transient voltage stability in transmission grids which is imperative to transmission stability and reliability. The last work evaluates modeling strategies and their impacts on the results of hosting capacity studies of DERs in transmission systems. These works highlight current shortcoming and ways for improvement and growth in traditional power system planning methods to accommodate these non-traditional

resources. The ultimate goals of this work and the integration of these resources are to sustainably, affordably, and reliably transform electrical grids to meet climate and national security goals.

Power System Planning for Sustainable, Reliable, and Accessible Electricity: Models, Methods, and Metrics

by

Phylicia Cicilio

A DISSERTATION

submitted to

Oregon State University

in partial fulfillment of
the requirements for the
degree of

Doctor of Philosophy

Presented March 4, 2020
Commencement June 2020

Doctor of Philosophy dissertation of Phylicia Cicilio presented on March 4, 2020.

APPROVED:

Major Professor, representing Electrical and Computer Engineering

---

Director of the School of Electrical Engineering and Computer Science

---

Dean of the Graduate School

I understand that my dissertation will become part of the permanent collection of Oregon State University libraries. My signature below authorizes release of my dissertation to any reader upon request.

Phylicia Cicilio, Author

ACKNOWLEDGEMENTS

I would like to give a special thank you to my advisor Dr. Eduardo Cotilla-Sanchez for his support and guidance, and for providing me the opportunity to pursue my degree at Oregon State University. His kindness, unrelenting support, and optimism have made graduate school a time of opportunity and excitement. He has pushed me academically beyond what I thought I was capable of doing, resulting in greater successes and higher self-esteem. He is someone who opens doors for those who don't even know those doors exist. He is a true asset to anyone who is lucky enough to have him as their advisor.

A special thank you to all the folks at Idaho National Laboratory, and especially Jake Gentle. I have learned so much from your guidance, grown from the opportunities you have provided, and most importantly learned how to truly think big.

I would like to thank the rest of the energy systems professors and graduate students. The community of this research group has been a huge source of support and friendship. The willingness of this group to share their expertise and time to assist in the success of myself and others has surpassed anything I could have expected.

To all my friends and my little family, Tony and Mozzarella, thank you for always believing in me.

Finally, I would like to thank my parents for all their love, compassion, and motivation. I am where I am today because of you.

CITATIONS

Material from this dissertation has been published in the following form:

Cicilio, P. and Orosz, M. and Mueller, A. and Cotilla-Sanchez, E., uGrid: Reliable Minigrid Design and Planning Toolset for Rural Electrification, IEEE Access, 2019

AND

Cicilio, P.and Cotilla-Sanchez, E., Evaluating Measurement-Based Dynamic Load Modeling Techniques and Metrics, IEEE Transactions on Power Systems, 2019

AND

Cicilio, P., Cotilla-Sanchez, E., and Gentle, J., Transient Voltage Stability Effects on Hosting Capacity of Behind-the-Meter Devices, in proceedings of IEEE Power and Energy Society General Meeting 2020

TABLE OF CONTENTS

TABLE OF CONTENTS (Continued)

Page

LIST OF FIGURES

LIST OF FIGURES (Continued)

Figure Page

LIST OF FIGURES (Continued)

Figure Page

LIST OF TABLES

LIST OF ALGORITHMS

LIST OF APPENDIX FIGURES

Chapter 1: Introduction

Electric grids are the most complex machines ever built. The birth of electrical grids in the United States occurred in 1882 in Manhattan, New York with a fossil-fuel generator in a direct current distribution system [13]. Over the past century and a half electric grids have grown into an intricate web of alternating current (AC) transmission and distribution systems with centralized generation largely based on high inertia fossil fuel and hydroelectric generation. Large regional electrical grid outages during the 20th century lead to federal regulation of the electric utilities as such outages caused significant economical and social harm [14]. Federal regulation brought operation and planning standards that must be met by utilities under penalty of fines. These operation and planning standards have historical been based on the traditional electrical grid model of centralized high inertia rotating mass generation.

The past four decades have brought rapid growth of renewable, decentralized, and non-rotating mass generation in electrical grids. In the United States this growth is largely due to state and federal policies incentivizing renewable energy research and deployment to reduce carbon emissions in light of climate change and to increase energy independence for national security. The relationship between the adoption of state renewable portfolio standard adoption and the growth of renewable energy consumption and reduction of fossil fuel and rotating mass generation by the electricity sector can be seen in Figures 1.1-1.2.

Both solar and wind energy experienced rapid growth at year 2000 and after while coal and petroleum decreased. The growth of consumption of hydroelectric and nuclear energy flatten during this time frame. Though hydroelectric and nuclear energy are not fossil fuel based they are shown grouped with the fossil fuel based resources due to their similar resource availability, electrical grid locations, and generating machine types. The fossil fuel, hydroelectric, and nuclear generators all use dispatchable resources and therefore are highly available and reliable sources of energy. Additionally, since their resources are all transported to the generation site these generators can be located anywhere in the system, with the exclusion of hydroelectric. Therefore, these generators, excluding hy-

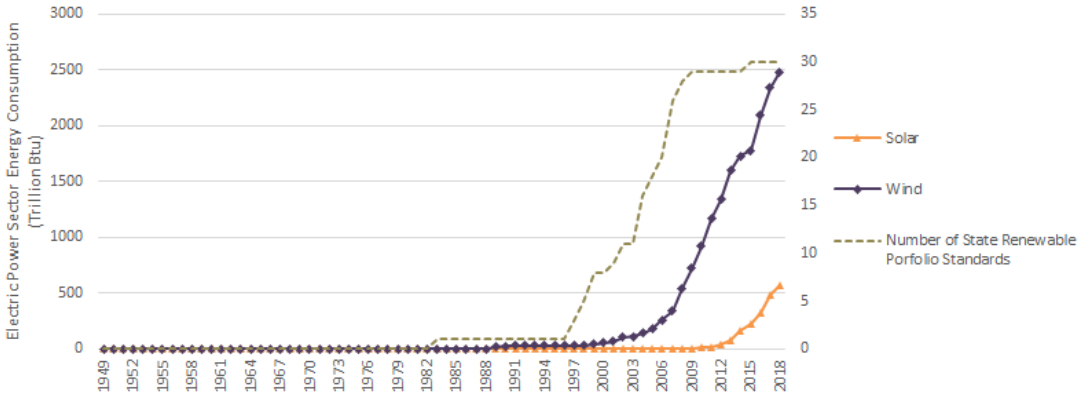

Figure 1.1: Electric Power Sector Energy Consumption of Renewable Energy Generation from 1949 to 2018 [1, 2]

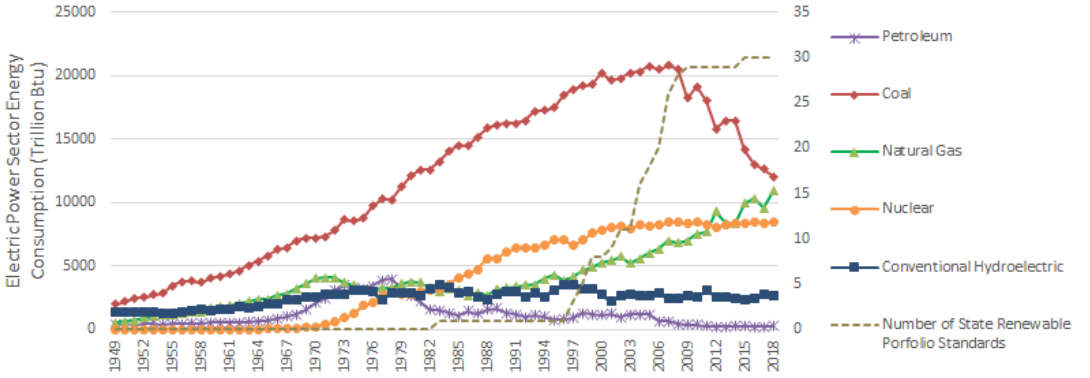

Figure 1.2: Electric Power Sector Energy Consumption of Fossil Fuel and Rotating Mass Energy Generation from 1949 to 2018 [1, 2]

droelectric, can be placed near population centers to reduce transmission losses between generation and consumption. All these generation types also use synchronous generators which have a rotating mass providing inertia to a synchronous AC electrical grid. Inertia is a critical grid resource which acts as a stabilizing force during disturbances on the grid such as unexpected transmission line or generating unit losses. This inertia acts as natural damping control to grid frequency. All of the traditional operation and planning standards were built around these assumptions of dispatchable, centralized, and high-inertia resources. Solar and wind are not dispatchable nor do they have a synchronously grid-connected rotating mass to provide inertia to the grid. This lack of

dispatchability is one cause of the increase in natural gas seen after 2000. Natural gas generation has a fast ramp rate which can help integrate these non-dispatchable variable resources. Solar and wind also need to be located where the resource is present, often placing these generation resources in remote locations distant from population centers. If the electrical grid infrastructure was built under the assumptions of non-dispatchable, decentralized, and no inertia resources the electrical grid, all connecting infrastructure, and operation and planning procedures and standards would all be designed to function well under these constraints. Instead the electrical grid is integrating resources which function and location are very different from what the system was built for. In comparison, you would not put diesel fuel into a gasoline car. The system here being the car was not designed to run on diesel fuel and the car will break. The question now is how do we transform our electrical grid infrastructure and operating and planning procedures and standards to stably, reliably, and affordably integrate these resources to meet our climate and national security goals.

This question is not unique to the United States. All nations, developed and developing, are faced with the same climate and national security challenges. For developing nations this challenge looks differently from developed nations due to less existing infrastructure. Here, another goal is increasing energy access through building new electrical grids either through transmission expansion or off-grid mini or microgrids. This goal is one of the 17 United Nations Sustainable Development Goals, as specified as Goal 7: Affordable and Clean Energy [15]. The affordability component is especially critical. A component not listed in the goal is reliability. Electricity reliability in developed electrical grids is a result of decades of learning from electrical grid outages and developing operation and planning procedures and standards to prevent them. This electricity reliability is taken for granted in most developed countries and is often taken as a guarantee. The value placed on reliability in the United States is now being tested as a result of multi-hour outages to prevent wildfires in California [16]. Public outcry has resulted from these outages confirming the great value that people of developed countries place on electricity reliability [16]. These types of electrical grid outages are a common occurrence in several developing countries. This is due to the high cost associated with the infrastructure, organizations, and policies needed to achieve such reliability. Therefore, achieving reliability in an affordable manner that matches the value that each society places on reliability is important and should be considered when addressing energy access, climate,

and national security goals.

This dissertation takes deep dives into how to transform the planning procedures and standards to achieve energy access, climate, and national security goals associated with the evolving resource mix. The second chapter addresses increasing energy access through development of off-grid minigrids. This work introduces an open-source planning tool which optimizes resource and equipment size and creates a distribution network placement map factoring in cost and reliability for minigrid development in partnership with Lesotho based company OnePower. Chapter three investigates the accuracy of measurement-based dynamic load modeling techniques used in transmission planning. Accurate dynamic load modeling is key to stable integration of distributed energy resources (DERs) such as solar and wind energy. This work highlights the need for improvements of these methods due to a lack of correlation between model accuracy and output response error. Chapter four draws the connection between dynamic loads and DERs. This chapter investigates the impact of dynamic loads and DERs on transient voltage stability in transmission grids. Transient voltage stability is necessary for stable and reliable operation of electrical grids and is assessed in planning procedures and regulated by federal regulating agencies. The fifth chapter calls for development of transmission hosting capacity studies of DERs and evaluates modeling strategies and their impacts on the results of hosting capacity studies. Hosting capacity studies determine the greatest amount of DERs that can be integrated into the system stably and reliably. These studies are commonly performed in distributed system and have yet to be performed in transmission systems. The conclusion of this dissertation covers the discovered highlights from each chapter and provides suggestions for continued efforts in these areas of research.

Chapter 2: uGrid: Reliable Minigrid Design and Planning Toolset for Rural Electrification

2.1 Introduction

Over one billion people globally lack access to electricity; of those, 84% live in remote areas [17]. The UNDP Sustainable Development Goal 7 ("Affordable and Clean Energy") aims to increase affordable and clean energy access for all [15]. Minigrids are one option for achieving this in remote communities where it is uneconomical to install transmission lines from a national electrical grid. It is estimated that 30% of newly electrified connections will be served by minigrids by 2030 [17] (up to 70% in rural areas [18]).

The goal of an energy service provider in deploying a minigrid, as for grid-connected utilities providing energy via a national grid, is to provide affordable and reliable electricity service to customers. Designing and planning a minigrid is a multi-phase project that includes (i) sizing of energy generation equipment and resource allocation, (ii) layout of the power distribution network, and (iii) incorporation of reliability cost-benefit analysis. Optimization is required at each stage to minimize the cost of electricity to the customer while maintaining an acceptable level of reliability. Industry standard tools to perform minigrid design, such as HOMER [19], are not free nor open source, typically providing fixed capabilities for an upfront fee and requiring additional fees for customized or added functionality (if available). Such tools can be financially infeasible for minigrid developers who operate within highly constrained budgets when aiming to provide a reasonable cost of electricity to customers in rural areas where operations costs are already much higher than those for grid-connected utilities operating in dense urban areas. In addition, in most cases the customer base of a minigrid has far less ability to pay than in productive urban environments. Free industry and academic tools exist, such as REopt Lite and DER-CAM among others [9, 10], however they are still proprietary, i.e., do not permit adaptability of the source code, which limits applicability in the context of evolving and highly variable off-grid markets. Alternately, open source tools are affordable and adaptable, and many open source tools are on par with licensed tools in terms of

functionality and capability [6].

A review of software designed for techno-economic optimization of hybrid energy systems (including HOMER, Hybrid2, RETScreen, iHOGA, INSEL, TRNSYS) is covered in [11] and [20], which also compares tool capabilities and limitations for PV hybrid system design. Tables 2.1-2.2 expand upon these works by including additional commonly used academic and industry standard tools and mature open-source minigrid development tools. Of note Switch, TEMOA, and OSeMOSYS are mature minigrid design open source tools generating results comparable to licensed tools [6] for certain tasks. The original uGrid tool, which forms the foundation of the work presented in this manuscript, is also included [8].

While the tools listed in Tables 2.1-2.2 address the issue of resource sizing and allocation, network layout design and reliability cost-benefit analysis represents a critical gap in the available minigrid development toolset. To the best knowledge of the authors the only tool that automates geographical distribution network layout for minigrids is ViPOR, created by NREL [21], which is no longer publicly available. There is therefore a pressing need for a network layout design tool with project level cost optimization capabilities.

Furthermore, network layout design is a prime opportunity for enhancing reliability. Unlike utilities where decisions are heavily influenced by amortizing costs of existing infrastructure, minigrid developers have an opportunity to use these metrics in actionable minigrid design. In rural electrification applications, however, there is a dearth of historical data from which to calculate reliability indexes to determine a cost benefit.

For utilities with established electrical grids that have such data gaps, probabilistic value-based analysis added to deterministic distribution planning criteria has been considered, e.g., for overhead distribution network planning, quantifying expected unserved energy availed as a cost (similar to EENS and ECOST) [22]. Distribution network layout has also been designed for high reliability through adding loops in existing systems to create meshed networks as a method for increasing reliability [23]. The idea of using a probabilistic value-based analysis is brought to rural electrification applications in [24, 25], which present the first distribution system planning model with topology decisions including reliability cost benefit (derived from N-1 line loss contingencies). However, this method does not provide geographical layout of the network as part of a publicly available tool.

Table 2.1: Minigrid Design Tools Part 1 [3–11]

Tool	Producer	Cost	Generation Types	Storage Types
HOMER	HOMER Energy	Free 3-week trial, 500–1500 USD	B, C, CHP, D, G, Gr, H, PV, Wi	FB, KiBAM, MKiBaM, PH, SSM
Hybrid2	NREL and University of Massachusetts	Free	D, PV, Wi	EKiBaM
Microgrid Design Toolkit	SNL	Free	PV, Wi, B, D, G	SMM
REopt	NREL	Not Available to Public	PV, Wi, B, Wa, G, D, FC	SMM
REopt Lite	NREL	Free	PV, Wi	SMM
DER-CAM	LBL	Free	CHP, D, G, Gr, PV, Wi	FB, SSM
MARKAL/TIMES	IEA-ETSAP	Costs 1275–3130 EUR to manipulate source code	B, C, CHP, D, G, Geo, Gr, GrS, H, N, PP, PV, T, Wa, Wi	SMM
RETScreen	Natural Resources Canada	Costs 869 CAD for 1 year, Free Viewer Mode	H, PV, G, B, D, H2, C, O, Wa	SMM
COMPOSE	Aalborg University	Free	B, C, CHP, G, Gr, PV, Wi	KiBaM
eTransport	SINTEF	Not Available	CHP, Gr, PP	SMM
MERIT	University of Strathclyde	Free	C, CHP, G, GrS, PV, Wi,	EKiBaM
MODEST	Optensys	Free	B, O, C, Wa, G, D, Wi	None
SimREN	iSUSI: Sustainable Solutions and Innovations	Not Available	Geo, H, PP PV, Wi	SMM
EnergyPLAN	Aalborg University	Free	B, C, CHP, D, G, Geo, Gr, GrS, H, N, PP, PV, T, Wa, Wi	CAES, PH, SSM
EnergyPRO	Aalborg University	3000+ EUR for all modules	B, C, CHP, D, G, Gr, H, PV, Wi	PH, SSM
iHOGA	Universidad Zaragoza	Educational Free, 500 EU for 1 year	D, G, Gr, H, PV, Wi	KiBAM, MKiBaM, SSM
Switch	Open Source	Free	C, N, H, Wi, PV, B, G	SMM
TEMOA	Open Source	Free	N, C, H, Wi, G, PV	SMM, CAES, PH
OSeMOSYS	Open Source	Free	C, N, H, D	PH, SSM
uGrid	Open Source	Free	PV, PP, CHP	FB

Key: Generation Types: Biomass (B); Coal (C); Combined heat and power (CHP); Diesel (D); Gas (G); Geothermal (Geo); Grid (Gr); Grid simple (GrS); Hydro (H); Hydrogen (H2); Nuclear (N); Generic power plant (PP), Photovoltaic (PV); Tidal (T); Wave (Wa); Wind (Wi). Storage Types: Compressed air energy storage (CAES); Extended kinetic battery (EKiBaM); Flow battery (FB); Kinetic battery (KiBaM); Modified kineticbattery (MKiBaM); Pumped hydro (PH); Simple storage (SSM).

Table 2.2: Minigrid Design Tools Part 2 [3–11]

Tool	Load Profile	Design Optimization	Reliability	Outputs
HOMER	Generator	F	Yes	A, E, EP, FA, FC, RP, SA,
Hybrid2	Generator	None	None	EP, FA, SA
Microgrid Design Toolkit	Input	F, R	Yes	FA, M, SA
REopt	Input and Generator	F	Yes	F, M, SA
REopt Lite	Input and Generator	F	Yes	F, M, SA
DER-CAM	Input	E, F	Yes	A, E, EP, FA, FC, SA
MARKAL/TIMES	Generator	F	None	E, EMI, EP, FA, FC, RP, SA,
RETScreen	Generator	F	None	F, M, SA
COMPOSE	Input	E, F	Yes	E, EP, FA, FC, SA
eTransport	Generator	F,E	None	E, EMI, EP, FA, FC, SA
MERIT	Generator	None	None	EP, FC, M, SA
MODEST	Generator	F	None	E,F,EP,M,SA,FA
SimREN	Generator	None	None	EMI, EP, SA
EnergyPLAN	Generator	None	None	E, EP, FA, FC, SA, RP
EnergyPRO	Generator	None	None	E, EMI, EP, FA, FC, SA
iHOGA	Generator	Single: F, Double or triple: combination of A, E, F, HDI, JC, NPC	None	A, E, EP, FA, FC, HDI, JC, RP, SA
Switch	Input	F	None	E, EMI, EP, FA, FC, RP, SA
TEMOA	Generator	F	None	E, EMI, EP, FA, FC, RP, SA
OSeMOSYS	Input and Generator	F	None	E, EMI, EP, FA, FC, RP, SA
uGrid	Input	F	None	FA, FC, SA

Key:
Design Optimization: Autonomy (A); Emissions (E); Financial (F); Human development index (HDI); Job creation (JC); Reliability (R).
Outputs: Autonomy (A); Emissions (E); Energy market interaction (EMI); Energy production (EP); Financial analysis (FA); Fuel consumption (FC); Human development index (HDI); Jobcreation (JC); Demands/supply match (M); Renewable penetration (RP); System analysis (SA)

The comparative review of available minigrid design tool capabilities supports a need for a holisitic approach that integrates equipment sizing and resource allocation, geographical distribution network layout, and reliability cost-benefit analysis. This work addresses this deficit by extending a coupled techno-economic minigrid development toolset, called uGrid, to integrate electricity distribution network layout optimization and reliability cost benefit analysis into the optimization. The original uGrid tool [8, 26] was developed primarily for optimized sizing and design of hybrid energy generation systems. The extended toolset builds on this base in collaboration with the minigrid developer OnePower to add capabilities lacking across the discipline and tuned to the minigrid development context of sub-Saharan Africa, where OnePower is based. This paper presents the extended open-source uGrid toolset.

The main contributions of this paper are summarized as follows:

- Present a holistic open-source minigrid toolset to simultaneously address optimization of sizing power generation equipment and distribution network layout optimization with incorporated cost-benefit reliability analysis.
- Present an improved control algorithm to the uGrid tool to minimize propane generator run-time and maximize the part load on the generator when it is in use. This is performed to reduce use of the generator at low-efficiency areas of the operation curve.
- Present a distribution network layout optimization method designed for flexible use in off-grid application. The optimization uses a Google Earth placemark file, geolocation of relevant community features, and economic/practical constraints to determine geographic utility pole placement, distribution wiring layout, and service drop wiring layout. A combination of Gaussian-mean clustering and network reduction is used to optimize pole placement and wiring layouts. The optimization includes cost-benefit analysis of N-1 contingency line-loss probability, called reliability probability, for improved network reliability.

The remainder of this paper is organized as follows: Section II briefly summarizes the uGrid minigrid design and planning toolset. Section III describes updates to the previously published uGrid equipment sizing and resource allocation tool that improves

the generation balance control algorithm. Section IV provides the network layout optimization formulation using Gaussian-mean clustering and network reduction used in the uGridNet tool. Section V presents a validation study, discussing the results of using the uGrid toolset for designing a minigrid for a reference community (the village of Ha Makebe, Lesotho). Section VI discusses the outcomes and contributions of the uGrid toolset for minigrid development and makes suggestions for future additions to the uGrid toolset.

2.2 uGrid Toolset Overview

The extended uGrid toolset is designed with accessibility in mind. The code base is built in Python which, in addition to having numerous available open source packages, also interfaces with industry standard tools such as Siemens PSS/E. Unlike other minigrid design tools which contain fixed and blackbox algorithms, the uGrid toolset is fully customizable. The optimization structure can be changed to perform multi-objective optimization, e.g., for emissions or fuel use minimization in addition to lowered cost. The project economic structure can be changed for specific location tax structures and project financial structure.

The uGrid toolset is comprised of two main tools: 1) equipment sizing and 2) network layout design. The inputs, outputs, and flow of information through the two tools are illustrated in Figure 2.1. The formulation and algorithms contained within the tools illustrated in Figure 2.1 are outlined in the following sections.

2.3 uGrid Resource Sizing and Allocation

The uGrid tool [8,26] optimizes the solar PV [kW] and battery [kWh] sizes (capital equipment) to best match the (statistical model of) expected load and the local solar resource, with a design availability target of 100% attained by recourse to a backup generator (fueled by, in this case study, propane). The uGrid tool uses particle swarm optimization (PSO) to select generation equipment sizing, co-optimizing (minimizing) the levelized cost of electricity for customers and fossil fuel use based on local Typical Meteorological Year (TMY) weather data, a yearly local load curve (5-15min discretization), equipment performance constraints, a control scheme minimizing generator run-time, and project

economics. Simulations are evaluated at hourly timesteps over one year, with power flows solved with DC power flow approximation (energy balance). This section updates the dispatch control strategy of the generators and battery storage during dusk and dawn hours to further optimize fuel usage (and associated CO_2 emissions).

The dispatch control of energy to/from generators and storage has significant impact on overall operating and maintenance costs, driven primarily by fuel usage in running the backup generator. In [27–29], the need for dispatch control algorithms that account for battery performance, lifespan, and time of day charging are discussed and developed, however these do not address issues related to the generator performance, in terms of fossil fuel usage or equipment stresses. The generation balance control algorithm presented in this paper comprehensively addresses battery performance, battery degradation as a function of lifetime use, time of day charging (i.e., source of energy for charging), maximized generator loading while running (for optimal fuel efficiency), and minimized generator startup demands/runtime (for reduced wear and reduced noise to households near the equipment). The following subsections outline the equations and procedure of the updated uGrid generation balance control algorithm.

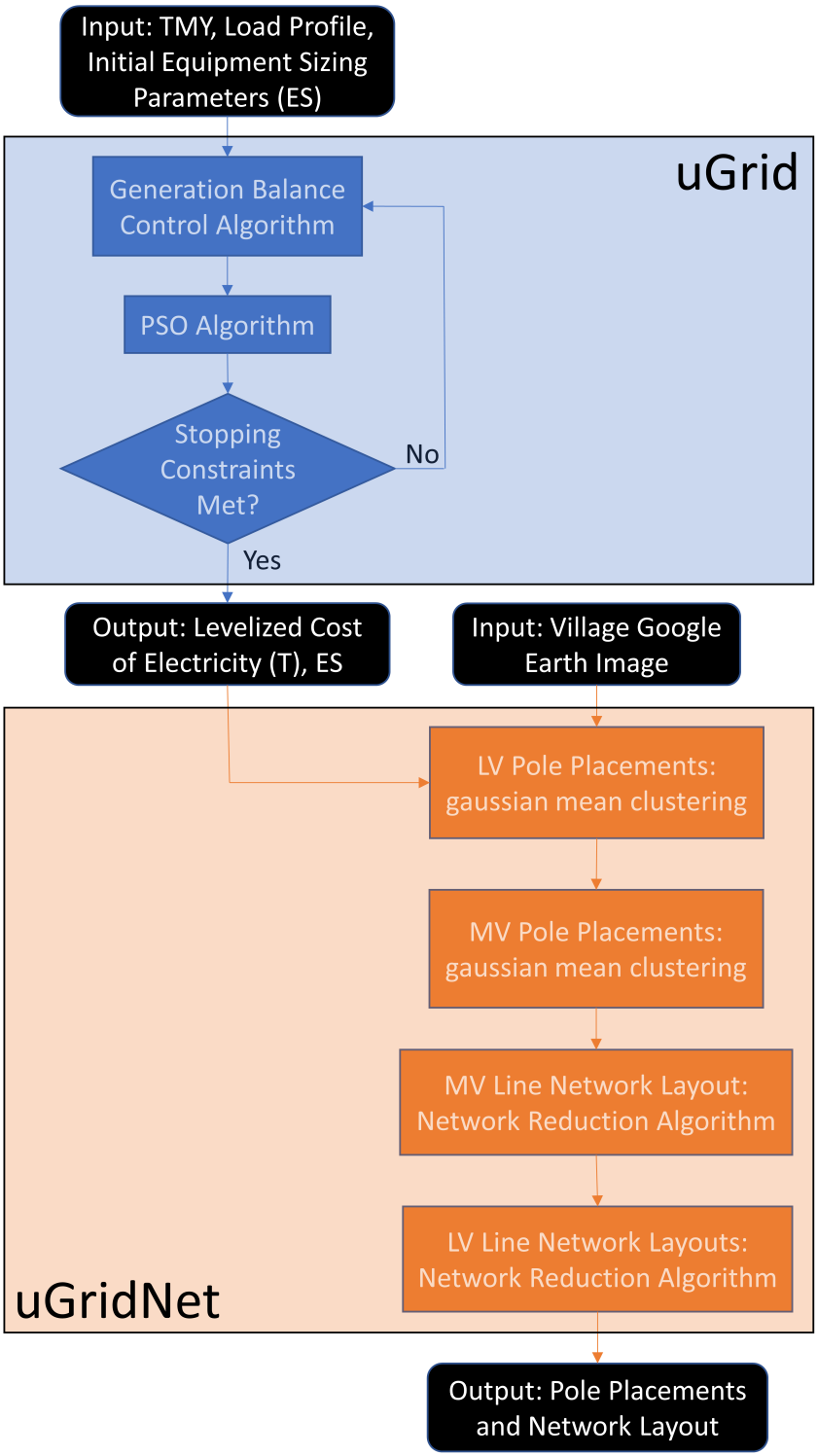

Figure 2.1: uGrid Toolset Flow Chart: The blue box denotes the key steps in the uGrid tool to perform resource allocation and sizing to calculate the levelized cost of electricity and equipment sizes (ES). The red box denotes the key steps in the uGridNet tool to perform distribution network layout and cost-benefit reliability to calculate the pole placement locations and network layout.

2.3.1 uGrid Model Parameters and Inputs

Table 2.3: Sets

H	set of time periods, indexed by hour h

Table 2.4: Parameters

PG_{load}	propane generator load demand
$PG_{partload}$	propane generator part load capacity
η_{PG}	propane generator part load capacity efficiency
PG_{Fuel}	propane generator fuel use for evaluated duration
PG_{kW}	propane generator size
P_{PG}	propane generator power flow
B_{kWh}	size of batteries
B_{temp}	battery temperature
$Limit_{Batt,charge}$	battery charging limit
$Limit_{Batt,discharge}$	battery discharging limit
SOC_h	state of charge of the battery
$P_{Batt,charge,h}$	available battery charge power for $h \in H$
$P_{Batt,discharge,h}$	available battery discharge power for $h \in H$
$P_{Batt,freespace}$	total available power battery charge
$P_{Batt,hightrip}$	battery power high trip limit
$P_{Batt,lowtrip}$	battery power low trip limit
$P_{Batt,h}$	battery power flow for $h \in H$
$P_{PV,h}$	solar PV power flow for $h \in H$
Loadleft	amount of load not served by solar PV power generation
$P_{dump,h}$	excess power generation that can't be stored in batteries or serve load for $h \in H$

Table 2.5: Inputs

L_h	local load profile for $h \in H$
L_{peak}	peak load demand
L_{kWh}	total load for the evaluated duration
TMY_h	typical meterological year weather data for $h \in H$
T_{amb}	ambient temperature

2.3.2 Fuel-based Electricity Generation

The propane generator is used as a backup for times when the load cannot be supplied by the solar PV generation and/or batteries. The generator is automatically sized for the maximum instantaneous load (with an added factor of safety) to ensure load is met 24/7 regardless of weather or any malfunctions of solar or battery equipment. Therefore the size of the generator is L_{peak}. The amount of propane consumed by the generator at any given hour is calculated from load demand on the generator and the part load efficiency [30]. Equations 2.1-2.3 calculate the fuel consumed for an hour of generation. Equation 2.2 is curve fitted to the part load efficiency data in [30].

$$PG_{partload} = \frac{P_{PG,h}}{L_{peak}} \tag{2.1}$$

$$\eta_{PG} = f(PG_{partload}) \tag{2.2}$$

$$PG_{fuel} = PG_{partload} * \eta_{PG} \tag{2.3}$$

2.3.3 Battery Storage

The batteries are present primarily to shift some fraction of daytime solar energy for nighttime use. The batteries are also charged by the propane generator when it would otherwise be running at a part load capacity, an approach that improves generator efficiency (which generally increases as load fraction increases). The batteries discharge,

providing power to the minigrid, when there is insufficient solar PV generation to meet the instantaneous load and the battery state of charge (SOC) is greater than the battery SOC lower limit (set to prevent equipment damage). The batteries are also subject to performance degradation due to temperature and lifetime charge/discharge cycling. The equations calculating battery performance and the algorithm determining battery power supply or storage (energy balance) are shown below.

$$\mathrm{P_{Batt,discharge}} = f(\mathrm{T_{amb}}, \mathrm{B_{kWh}}) \tag{2.4}$$

$$\mathrm{SOC}_h = \mathrm{SOC}_{h-1} - \mathrm{P_{Batt,discharge}} \tag{2.5}$$

$$\eta_{\mathrm{Batt,temp}} = f(\mathrm{T_{amb}}) \tag{2.6}$$

$$\mathrm{P_{Batt,hightrip}} = \mathrm{Limit_{Batt,high}} * \mathrm{B_{kWh}} * \eta_{\mathrm{Batt,temp}} \tag{2.7}$$

$$\mathrm{P_{Batt,lowtrip}} = \mathrm{Limit_{Batt,low}} * \mathrm{B_{kW}} * \eta_{\mathrm{Batt,temp}} \tag{2.8}$$

$$\mathrm{P_{Batt,freespace}} = \mathrm{B_{kWh}} * \eta_{\mathrm{Batt,temp}} - \mathrm{SOC}_h \tag{2.9}$$

$$\mathrm{P_{Batt,charge}} = \min(\mathrm{Limit_{Batt,Charge}}, \mathrm{P_{Batt,freespace}}) \tag{2.10}$$

$$\mathrm{P_{Batt,discharge}} = \min(\mathrm{Limit_{Batt,Discharge}}, (\mathrm{SOC}_h - \mathrm{P_{Batt,lowtrip}}) \tag{2.11}$$

Equation 2.4 calculates how much energy is consumed in the battery due to self discharge over the hour interval; this is subtracted from the state of charge of the battery in Equation 2.5. The battery efficiency due to temperature is accounted for in both the battery high power limit and the amount of storage capacity left in the battery in Equations 2.7 and 2.9 respectively. The maximum amount of energy that can be supplied by the battery during the hour time period is determined in Equation 2.11, and the maximum amount of energy that can be stored is determined with Equation 2.10.

The amount of energy flowing into or out of the battery is determined in Procedure 1 outlined in the following section.

2.3.4 Control

The control algorithm determines whether the propane generator should be running and if so at what capacity. This determination is based on the instantaneous and projected load demand and the battery SOC. The control algorithm also maximizes solar energy use by prioritizing battery charging during the day (as opposed to charging via generator) and only allowing discharging of the batteries when solar insolation is insufficient to supply loads (i.e., from evening to early morning and in cases of inclement weather where clouds reduce insolation). This updates the previous approach which restricted battery use to nighttime hours which had an unintended side effect of promoting excess generator use during early morning daytime. The new approach reduces the number of times the propane generator will turn on per day, reducing wear on the generator.

The nighttime control schema is achieved by forecasting the kWh of demand expected over the following night (approx. 12 hours), termed *LoadLeft* (i.e., load demand remaining to be served before solar generation comes online the following morning). This forecasting is based on a statistical model for demand, created from historically collected data, and is a function of time of year and the particular community being served (number and type of connections), as presented in previous publications [8]. The generator is engaged when it is determined that the battery SOC is insufficient to meet the forecasted nighttime demand for the residual period until solar generation comes back online. Once the generator is turned on, in addition to serving instantaneous demand it is also used to charge batteries at the maximum rate allowable (by the battery chemistry) to maximize part load efficiency of the generator. The generator is turned off when the battery SOC is sufficient to meet the forecasted load. If *LoadLeft* is accurate, the generator will turn on a maximum of once per 24 hours and, if it does, will ensure the batteries are charged up to the level required to meet demand through the night (until morning solar insolation is sufficient to supply the load).

The power flows from the battery and generators are determined by the decision flow chart shown in Procedure 1.

An example of a single day of power flows from the month of July in Lesotho and

Procedure 1 Generation Balance Control, providing the controls decisions for when the batteries are charged or discharged and when the propane generator will dispatch. The parameters are described in Tables 2.3-2.5.

Input: $P_{PV,h}$, $P_{Batt,charge,h}$ $P_{Batt,discharge,h}$, $P_{Batt,freespace}$, SOC_h, LoadLeft, DayHour
Output: SOC_h,$P_{Batt,h}$, $P_{PG,h}$,
for $h \leftarrow 0$ to H **do**
  if $P_{PV,h} > 0$ **then**
    if $P_{PV,h} - L_h < 0$ **then**
      if $P_{Batt,freespace} >$ LoadLeft AND $P_{Batt,discharge,h} > L_h$ **then**
        $P_{PG,h} \leftarrow 0$ $P_{Batt,h} \leftarrow L_h$ - $P_{PV,h}$ $P_{dump,h} \leftarrow 0$
      else
        $P_{PG,h} \leftarrow min(PG_{kW},(L_h - P_{PV,h} + P_{Batt,charge,h}))$ $P_{Batt,h} \leftarrow -(P_{PG,h} + P_{PV,h} - L_h)$ $P_{dump,h} \leftarrow 0$
      end if
    else
      $P_{PG,h} \leftarrow 0$ $P_{Batt,h} \leftarrow -min((P_{PV,h} - L_h),P_{Batt,charge,h})$ $P_{dump,h} \leftarrow P_{PV,h} + P_{Batt,h} - L_h$
    end if
  else
    if $P_{Batt,freespace} >$ LoadLeft AND $P_{Batt,discharge,h} > L_h$ **then**
      $P_{PG,h} \leftarrow 0$ $P_{Batt,h} \leftarrow L_h$ $P_{dump,h} \leftarrow 0$
    else
      $P_{PG,h} \leftarrow min(PG_{kW},(L_h + P_{Batt,charge,h}))$ $P_{Batt,h} \leftarrow -(P_{PG,h} - L_h)$ $P_{dump,h} \leftarrow 0$
    end if
  end if
end for

battery state of charge (SOC) including the load profile using the control algorithm covered in this section is shown in Figures 2.2-2.3.

As can be seen in Figure 2.2, the propane generator is used minimally and only when there is insufficient solar PV generation or battery charge. Note: power flow from the battery never exceeds charging/discharging limits.

2.3.5 Model Outputs

The output from the uGrid tool is a spreadsheet containing the resulting capital equipment sizes (kW of PV and kWh of batteries) and corresponding projected levelized cost of electricity (LCOE). Future work includes developing a graphical user interface (GUI) to increase ease of use of the tool. Additionally, other future improvements to the tool could include performing a complexity calculation to compare the tool's run-time to other available tools, considerations for load growth, and additional power generation sources such as wind and small scale hydro power where resource input data is available (in comparison with solar resource data, location-specific data for assessing yield and financial

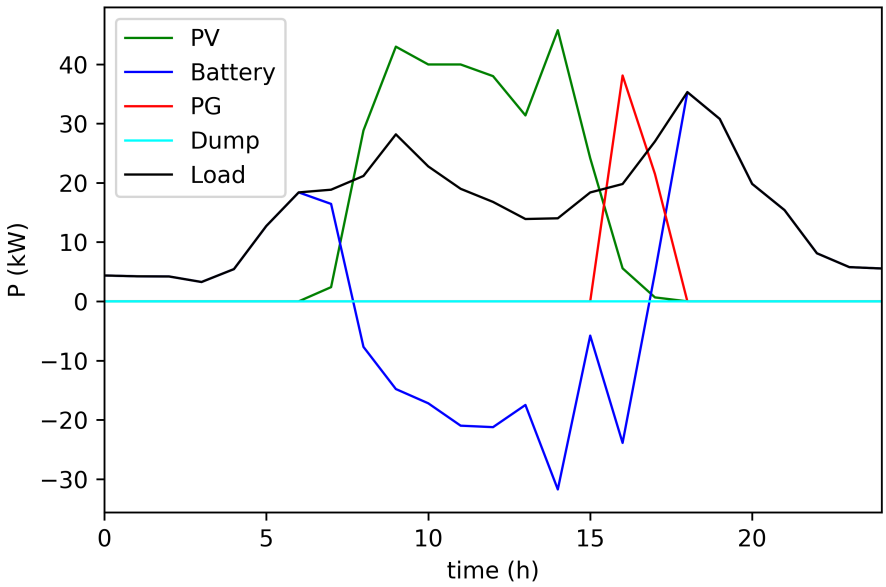

Figure 2.2: Example Day Power Flows: A single day's power flows from the month of July in Lesotho is plotted highlighting the power outputs at each hourly timestep from each of the generation equipment and the load demand.

viability of wind and hydro generation is relatively more dependent on local survey and measurement campaigns), and AC steady state and dynamic power flow analysis.

2.4 uGrid Net Formulation

The uGridNet tool optimizes the AC distribution grid layout to reduce the cost of the distribution equipment while including a reliability cost benefit. The uGridNet tool's main input is a Google Earth placemark file of the community to be electrified, with the houses, roads, and other non-buildable areas (e.g., areas identified in site surveys or Environmental and Social Impact Assessments or Management Plans as culturally, historically, archaeologically, or ecologically sensitive) highlighted as exclusion zones. Other inputs include the GPS locations of the structures to be connected to the grid, the GPS location of the generation equipment, and the desired voltage levels of the grid. The uGridNet network layout has a medium voltage (MV) line network backbone

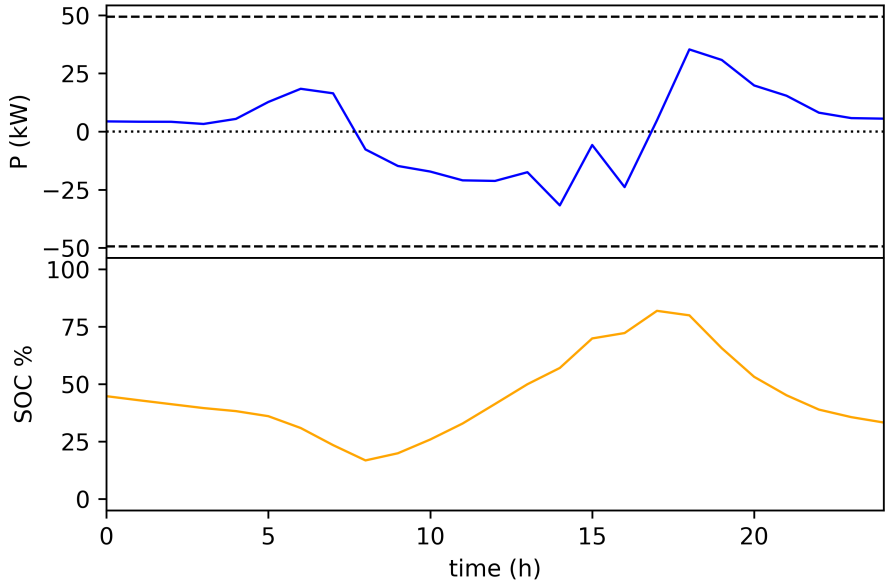

Figure 2.3: Example Day Battery Power Flow with State of Charge of Battery: The black dashed lines denote the charging and discharging limits on the battery. The battery power flow is negative when it is charging (storing power from the PV or fuel-based generation) and positive when it is discharging (providing power to the minigrid).

that connects low voltage (LV) line networks. The default voltage levels in uGridNet are 6.3kV (MV) and 220V (LV), which conform to regional standard and are realistic ratings of the lines for the current load levels to be carried in typical community-scale systems. The LV network connects to the customers with service drops.

Constraints for maximum line capacity must be respected when determining how many nodes are on each LV line network; for this purpose the load demand for each household (or business or institution) is set at its expected peak load. This power system constraint is built into the network reduction algorithm described in more detail below.

Based on these data and constraints, uGridNet generates optimized pole placement, MV line network layout, LV line network layout, service drop connections to LV line networks, and cost. The cost includes a reliability cost-benefit, motivated by the works of [3, 25, 31]. The uGridNet tool uses network layout with N-1 line loss contingencies

to determine lost load from contingencies, from which the lost revenue for the minigrid developer is calculated. This provides the minigrid developer an economic incentive to consider reliability in network design despite an increased initial cost due to additional lines.

2.4.1 uGridNet Methods

The uGridNet tool uses two methods to complete the network layout design: Gaussian-mean clustering (for pole placement) and a network reduction algorithm (for network layout, see Procedure 2). Figure 2.1 illustrates the process flow of the uGridNet tool. The Gaussian-mean clustering algorithm is from the publicly available scikit Python package GaussianMixture [32]; GaussianMixture is the fastest algorithm for learning mixture models [32].

Procedure 2 Network Reduction, where t_{repair} is the estimated time to repair any line loss contingency (must be determined by the user) and p is the user-selected reliability probability (ranging from 0-100%).

Input: Pole Placements, p, t_{repair}, LCOE, EC
Output: Total network cost, wiring layout
Calculate distances between all poles
Sort connections between all poles by length, longest to shortest
Create initial solution:
    Wiring solution ← Set all poles connected to each other
    Calculate initial total network cost
for $n \leftarrow 0$ to N **do**
    Remove n line from the wiring solution
    Calculate number of islands in wiring solution
    if number of islands in wiring solution > **then**
        Add n line back to the wiring solution
    else
        Calculate total network cost
        if total network cost > best total network cost **then**
            Add n line back to the wiring solution
        end if
    end if
end for

The network layout algorithm begins with a fully connected network. Here lines are considered for removal from longest (most expensive) to shortest. However, the order of consideration for removal is important and if changed will change the end result; there is therefore room for improvement if other order-determining heuristics are of interest. For each line in that network then, the line is removed if no islands are created and

if the total cost of the network (the combined cost of the network equipment and the reliability cost as seen in Equation 2.12) is lowered by removing that line. Finding connected components, a theory used in graph theory, is used to verify that removing a line in the network does not create islands within the minigrid.

$$\begin{aligned}&\text{Total Network Cost} = \\ &\quad \text{Network Equipment Cost} + \text{Reliability Cost}\end{aligned} \tag{2.12}$$

(a) (b) (c)

Figure 2.4: (a) Google Earth U.S. town image, (b) with exclusion zones, such as houses and roads and rivers, highlighted in white, (c) house locations as located on the image

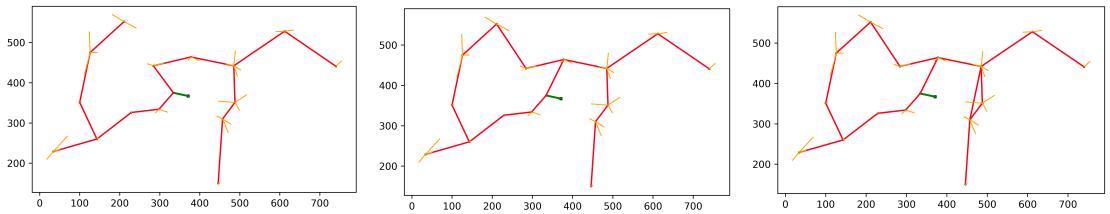

(a) 0% (b) 25% (c) 100%

Figure 2.5: U.S. town network solution with (a) 0%, (b) 25%, and (c) 100% reliability probability: The red lines denote the LV distribution network lines and the green line denotes the MV distribution network line. The yellow lines denote the lines to connect the houses to the LV distribution network. The black dot denotes where the generation station point of connection is located.

The equipment cost includes poles, transformers, and distribution boxes and is a function of the length and voltage rating of the power lines; regional costs for equipment components are input by the user. The reliability cost is the cost of the potential loss of service (load) due to the outage or loss of any line in the system, determined by Equation

2.13:

$$\text{Reliability Cost} = \sum_{n=1}^{N} p * \text{L}_{\text{loss},n} * t_{\text{repair}} * \text{LCOE} \tag{2.13}$$

where LCOE is from the uGrid tool, p is the reliability probability which is the probability of the line loss, and t_{repair} is as defined above. The load loss due to a line loss, denoted as $\text{L}_{\text{loss},n}$ in Equation 2.13, is calculated using the connected components method from graph theory as described earlier (identifies customer points islanded by the line loss).

Without considering a reliability cost, the lowest cost network will have the fewest number of lines that connects all nodes. From a graph theory perspective, this lowest cost network will be a radial network. Adding a reliability cost from the reliability cost-benefit analysis (N-1 line loss contingencies) results in partially meshed networks. The greater the reliability cost, the more meshed the network will become. Therefore, if any of the variables in Equation 2.13 are increased, the network will become more meshed due to the presence of more lines in the network (illustrated in the following section case studies). Note, however, that costs of any potentially required protection or switching equipment for network meshing are not yet considered in this algorithm.

Areas for further development of the uGridNet tool include adding ability to prefer line layout to follow along roads/walkways, considerations for (resiliency in cases of) load growth, and additional costing that may be associated with network meshing.

2.4.1.1 Network Layout Design Benchmark

The uGridNet code was first benchmarked on a small town in the United States to verify that the generated network layout out was reasonable in comparison to how electrical grid network layouts are implemented in the United States. Though the GPS location of the town and relative house placements reflect the actual community in the United States, all other inputs to the uGridNet tool (load demand, line voltage ratings, etc.) were set to reflect a minigrid being built for rural electrification in Lesotho (to provide an "apples-to-apples" comparison to the Ha Makebe, Lesotho study in Section V). The LV and MV line voltage rates were chosen to be 220V and 6.3kV respectively.

The input to uGridNet was the Google Earth placemark file of the small town in the

United States with marked exclusion zones, as seen in Figure 2.4(b). For comparison, the original Google Earth placemark file without the marked exclusion zones is seen in Figure 2.4(a). The GPS locations of the 31 houses to be connected and the location of the generation equipment were also provided.

The output from uGridNet (Figures 2.5(a)-2.5(c)) shows the medium voltage line in green, the low voltage lines in red, the housing connections in orange, and the generation location with a black dot. In these three figures, the reliability probability (p) was set sequentially to 0%, 25%, and 100% to illustrate the effects of the reliability cost benefit analysis, and the network layouts become more meshed as reliability probability increases.

At 100% probability, the network is still only partially meshed. This is because a fully meshed network would only be a result of accepting networks with zero reliability cost and no allowed load loss (with an obvious trade-off of increased capital cost). In this method, however, load loss from N-1 line loss contingencies are allowed, with the reliability cost included in the total cost. Note that the same effect (increasing mesh) would be seen if any of the variables in the reliability cost were increased (not just p). The appropriate amount of reliability cost to include depends on the reliability expectations of the customers (which may be assessed through surveys) and total budget constraints.

In the United States there is a high electrical reliability expectation, which should logically correspond to higher reliability costs (more meshing), however a typical US town's distributed grid actually looks more similar to the fully radial network in the 0% reliability probability result (Figure 2.5(a)). This is because US electrical grids achieve high reliability standards in more ways than just increasing mesh. When taking this into consideration, we can conclude that Figure 2.5(a) demonstrates a realistic looking electrical grid network that could theoretically exist in the United States.

2.5 Ha Makebe, Lesotho Case Study

The uGrid toolset is built for designing and planning minigrids in sub-Saharan Africa by OnePower. The village of Ha Makebe, Lesotho is the first village where they are building a community minigrid. This section provides the results of using the combined uGrid toolset for designing the Ha Makebe minigrid.

The key inputs and outputs of the uGrid tool for Ha Makebe are shown in Table 2.6.

Table 2.6: Sample uGrid Inputs and Outputs for Ha Makebe

Number of houses	212
Village peak load	37.4 kW
Battery size	215 kWh
Solar PV size	100 kW
Propane generator size	45 kW
Levelized cost of electricity	0.35 $/kWh

The power flow outputs from the uGrid tool for Ha Makebe for the months of February and July (southern hemisphere summer and winter, respectively) are shown in Figures 2.6 and 2.2 (above). From these two figures it can be seen that in the winter months the propane generator is used more (as expected with lower solar insolation but similar or increased loads, e.g., due to heating).

The levelized cost of electricity generated from the uGrid tool is used as input to the uGridNet tool. The Google Earth placemark files of the Ha Makebe village (raw and with exclusion zones) and the locations of the houses to be electrified are seen in Figures 2.7(a)-2.7(c).

Figures 2.8(a)-2.8(d) show the locations of the poles and network layout for three reliability probability cases (0%, 10%, 25%). As expected, increasing reliability probability results in more network meshing. In order to select between these cases, the minigrid developer must determine a target reliability probability, something which remains challenging due to the lack of historical data on the likelihood of line losses in minigrids. Evaluating how the reliability costs compare to the equipment costs gives perspective. A comparison of the associated equipment and reliability costs for the networks with 0%, 10%, 25%, and 100% reliability probability are reported in Table 2.7.

As seen in Table 2.7, as the reliability probability increases from 10% to 100% the reliability cost increases from 15% to 55% of the total cost of the system used in the network reduction algorithm. Evaluating the reliability cost as a percent of the total cost could help provide insight to minigrid developers to determine an appropriate amount of reliability probability to use.

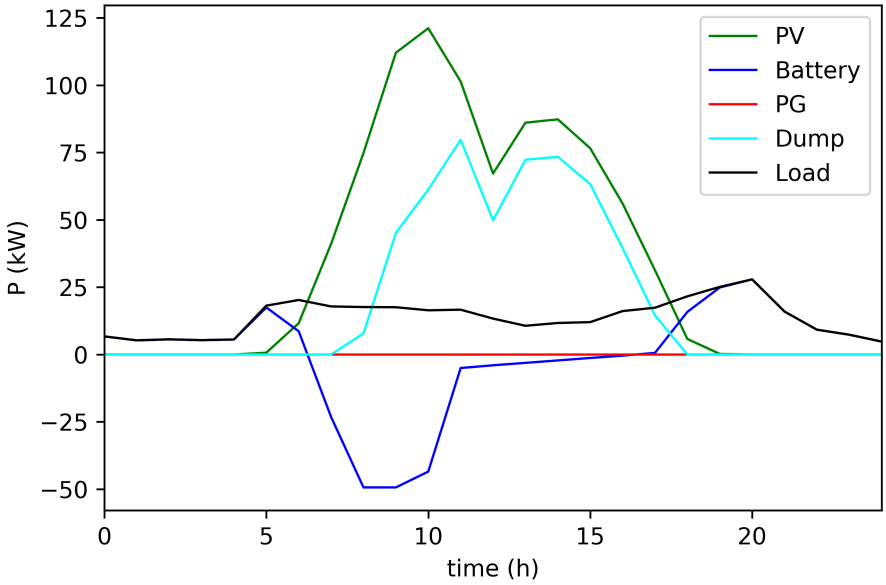

Figure 2.6: Ha Makebe single day February power flows are plotted, highlighting the power outputs at each hourly timestep from each of the generation equipment and the load demand.

(a) (b) (c)

Figure 2.7: (a) Google Earth Ha Makebe image, (b) with exclusion zones, such as houses and roads and rivers, highlighted in white, (c) house locations as located on the image

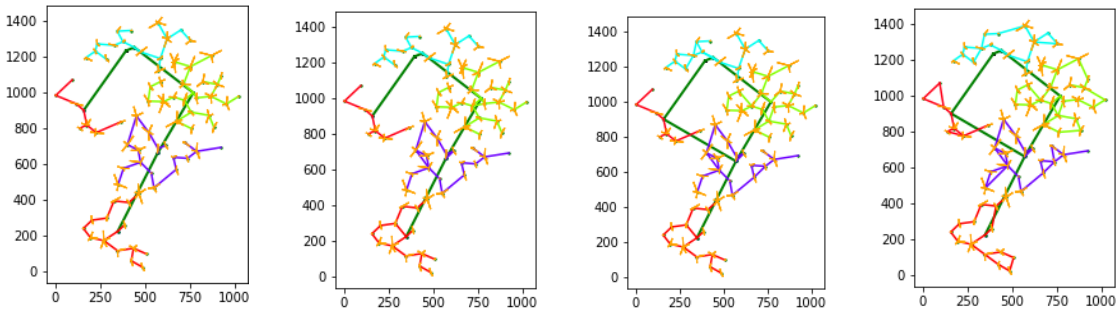

(a) 0% (b) 10% (c) 25% (d) 100%

Figure 2.8: Ha Makebe network solution with (a) 0%, (b) 10%, (c) 25%, and (d) 100% reliability probability: The bold dark green lines denote the MV distribution network lines. The thin yellow lines denote the lines to connect the houses to the LV distribution network. The LV distribution network are the multicolored lines. Each color denotes a separate grouping of LV distribution lines which connect to the MV distribution network where seen. The black dot denotes where the generation station point of connection is located.

Table 2.7: Reliability and equipment costs associated with the networks solutions for 0%, 10%, 25%, and 100% reliability probability of the Ha Makebe village.

Reliability Probability	Reliability Cost	Total Cost
0%	$0	$20,709
10%	$3,691	$24,491
25%	$6,620	$27,800
100%	$26,500	$47,600

2.6 Conclusions and Future Work

This paper introduces an extended holistic open-source minigrid planning and design toolset called uGrid. To the best knowledge of the authors, there are no other toolsets that integrate equipment sizing, geographical distribution network layout, and reliability cost-benefit analysis for the design of islanded minigrid power systems. The toolset consists of uGrid, a techno-economic resource sizing tool, and uGridNet, a network layout design tool. Here we present an updated control algorithm that minimizes propane generator wear, maximizes generator efficiency, and minimizes fossil fuel usage. The uGridNet tool uses an inputted Google Earth placemark file of the village and generates optimized pole placement, connection wiring layout, and distribution wiring layout. A

combination of Gaussian-mean clustering and network reduction is used to optimize pole placement and wiring layouts, including cost-benefit analysis of N-1 contingency line-loss probability for improved network reliability.

The tool is demonstrated through design of a minigrid for the community of Ha Makebe, Lesotho. The developed LV and MV network layouts based on varying levels of desired reliability provide guidance for design of the system and point to the need for collection of reliability metrics to inform future design decisions.

This toolset fills a gap for flexible and affordable holistic minigrid planning, needed by minigrid developers. The toolset is designed for continued improvement and community input and is readily accessible through the open-source platform GitHub [33]. Areas for future expansion include: integrating additional resource types (e.g., wind and hydro) to the uGrid tool, adding steady state and dynamic power flow analysis, providing considerations for network layout to follow along roads and walkways, projecting for expected load growth (in both resource sizing and network layout), and adding a complexity calculation comparing the tool's run-time in comparison to similar tools.

Chapter 3: Evaluating Measurement-Based Dynamic Load Modeling Techniques and Metrics

3.1 Introduction

The introduction of phasor measurement units (PMUs) and advanced metering infrastructure (AMI) has ushered in the era of big data to electrical utilities. The ability to capture high-resolution data from the electrical grid during disturbances enables the more widespread use of measurement-based estimation techniques for validation of dynamic models such as loads. Transient stability studies use dynamic load models. These studies are key for ensuring electrical grid reliability and are leveraged for planning and operation purposes [34]. It is imperative that dynamic load models be as representative of the load behavior as possible to ensure that transient stability study results are accurate and useful. However, developing dynamic load models is challenging, as they attempt to represent uncertain and changing physical and human systems in an aggregate model.

Several methods exist for determining load model parameters, such as measurement-based techniques using power systems sensor data [35–40], and methods that use parameter sensitivities and trajectory sensitivities [35, 37, 41–43]. A common practice in measurement-based techniques is to use system response outputs, such as bus voltage magnitude, from PMU data and simulation data and compare the output with a similarity measure, such as Euclidean distance. The error between PMU data and simulation output is referred to as response error in this paper. As investigated in [12], the underlying assumption that reducing response error results in a more accurate model and system is not guaranteed.

This paper examines the relationship between response error and system and model accuracy to highlight concerns with common measurement-based technique practices. The methods used in the study examine whether the selection of a load model is accurate at a given bus. Measurement-based techniques typically perform dynamic load model parameter tuning to improve accuracy. In parameter tuning, significant inter-dependencies and sensitivities exist between many dynamic load model parameters [35, 37, 41–43],

which is one of the reasons why dynamic load model parameter tuning is challenging. This study compares the selection of two loads models, the dynamic composite load model (CLM) and the static ZIP model instead of parameter tuning. The static ZIP model is the default load model chosen by power system simulators and represents loads with constant impedance, current, and power. The CLM load model has become an industry standard, particularly for the western United States, which represents aggregate loads including induction machine motor models, the ZIP model, and power electronics [38, 44]. The choice of changing the load model is made to compare known differences in responses from load motor models with the CLM model and static load models with the ZIP model. By comparing load model selection, the presence of a correlation between response error and system accuracy will be assessed.

This study performs two experiments to address two main hypotheses. The first experiment is a system level experiment to test hypothesis 1) can response error determine the total system accuracy of how many load models at buses in the system are accurate? The second experiment is a bus level experiment to test hypothesis 2) can response error indicate if a load model being used at a bus is accurate? The results from these experiments demonstrate that it can't be assumed that response error and system accuracy are correlated. The main contribution of this paper is to identify the need for validation of techniques and metrics used in dynamic load modeling, as frequently used metrics can deliver inaccurate and meaningless results.

The remainder of this paper is organized as follows. Section II discusses the use of dynamic load models in industry and those used in this paper. In Section III, similarity measures are discussed in relevance to power systems time series data. Section IV details the methodology used to evaluate the system level experiment of hypothesis 1. Section V provides and discusses the results from system level experiment. Section VI details the methodology used to evaluate the bus level experiment of hypothesis 2. These results are provided and discussed in Section VII. In conclusion, Section VIII discusses the implication of the results found in this study and calls for attention to the importance of careful selection and validation of measurement-based technique metrics.

Table 3.1: Examples of amplitude and time shifting and stretching [12]

	Amplitude	**Time**
Shift	initialization differences, discontinuities	different/unknown initialization time
Stretch	noise	oscillations at different frequencies

3.2 Similarity Measures

A similarity measure compares how similar data objects, such as time series vectors, are to each other. A key component of measurement-based techniques is to use a similarity measure to calculate the response error. Then typically, an optimization or machine learning algorithm reduces this response error to improve the models or parameters in the system. Several measurement-based dynamic load model estimation studies employ Euclidean distance as a similarity measure [38,45,46] . However, there are characteristics of power systems time series data which should be ignored or not emphasized, such as noise, which are instead captured by Euclidean distance. Power system time series data characteristics include noise, initialization differences, and oscillations at different frequencies. These characteristics result in shifts and stretches in output amplitude and time as detailed in Table 3.1.

The characteristics listed in Table 3.1 are the effect of specific phenomena in the system. For example, differences in control parameters in motor models and potentially also playback between motor models can cause oscillations at different frequencies. Certain changes in output are important to capture as they have reliability consequences to utilities. An increase in the initial voltage swing after a disturbance can trip protection equipment. An increase in the time it takes for the frequency to cross or return to 60 Hz in the United States has regulatory consequences resulting in fines. Response error produced by similarity measures should capture these important changes. Other changes to output, such as noise, should be ignored.

Different situations when comparing simulation data to simulation data versus comparing simulation data to PMU data cause some characteristics listed in Table 3.1. Comparing simulation data to simulation data occurs in theoretical studies, and comparing simulation data to PMU data would be the application for utilities. Initialization differences and differences in initialization time can occur when comparing simulation data

to PMU data due to the difficulty in perfectly matching steady-state values. However, when comparing simulation data to simulation data, initialization differences and differences in initialization time likely highlight errors in the simulation models, parameters, or values.

Similarity measures have the capability to be invariant to time shift and stretch or amplitude shift and stretch. Table 3.2 lists the similarity measures examined in this study with their corresponding capabilities. These similarity measures are chosen to test the sensitivities to all four quadrants of Table 3.1.

Table 3.2: Similarity measures capabilities

	Amplitude Shift	**Amplitude Stretch**	**Time Shift**	**Time Stretch**
Euclidean Distance				
Manhattan Distance				
Dynamic Time Warping			•	•
Cosine Distance	•			
Correlation Coefficient	•	•		

Euclidean distance and Manhattan distance are norm-based measures which are variant to time and amplitude shifting and stretching. Euclidean distance is one of the most commonly used similarity measures in measurement-based techniques. These norm based distances can range from 0 to ∞.

The cosine similarity takes the cosine of the angle between the two vectors to determine the similarity. By only using the angle between the vectors, this similarity is invariant to amplitude shifting [12]. This similarity can range from -1 to 1.

The Pearson correlation coefficient is invariant to amplitude shifting and stretching and also ranges from -1 to 1 [12].

Dynamic time warping (DTW) identifies the path between two vectors of the lowest cumulative Euclidean distance by shifting the time axis. DTW is invariant to local and global time shifting and stretching [46]. The DTW algorithm used in this study is only invariant to time shifting. DTW can range from 0 to ∞.

Figure 3.1 and 3.2 show how amplitude and time shifting and stretching affect the error produced by similarity measures. The time series plots in Figure 3.1 show a sine wave with corresponding amplitude or time shift or stretch. The similarity measures

calculate the difference between each of the time series subplots. The error generated for each similarity measure is normalized for comparison. The error is normalized separately for each similarity measure, so the sum of the error from the amplitude and time shift and stretch sums to one. Figure 3.2 compares the error results from each of the subplot scenarios.

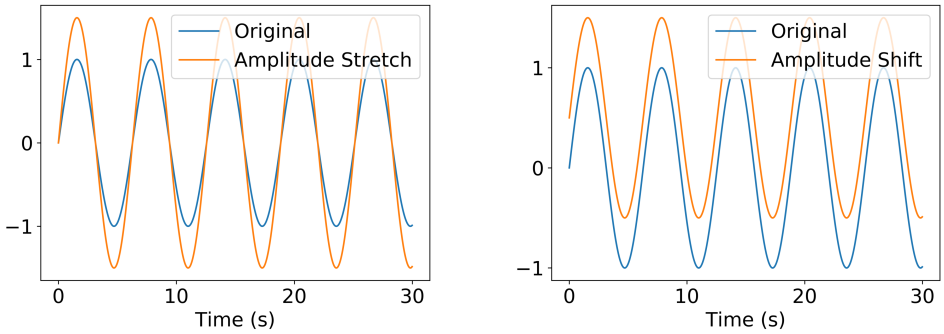

(a) Amplitude stretch

(b) Amplitude shift

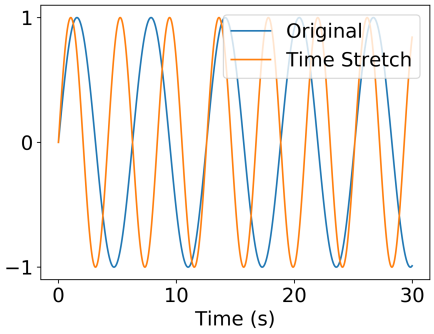

(c) Time Stretch

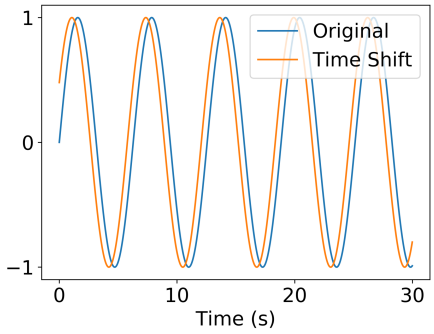

(d) Time Shift

Figure 3.1: Example time series with amplitude and time shift and stretch

The results in Figure 3.2 demonstrate the abilities of each similarity measure. The similarity measures are denoted as: Euclidean distance (ED), Manhattan distance (MH), dynamic time warping (DTW), cosine distance (COS), and correlation coefficient (COR). Correlation coefficient has negligible error produced with both amplitude shift and stretch. Cosine distance has negligible error with amplitude stretch. Dynamic time

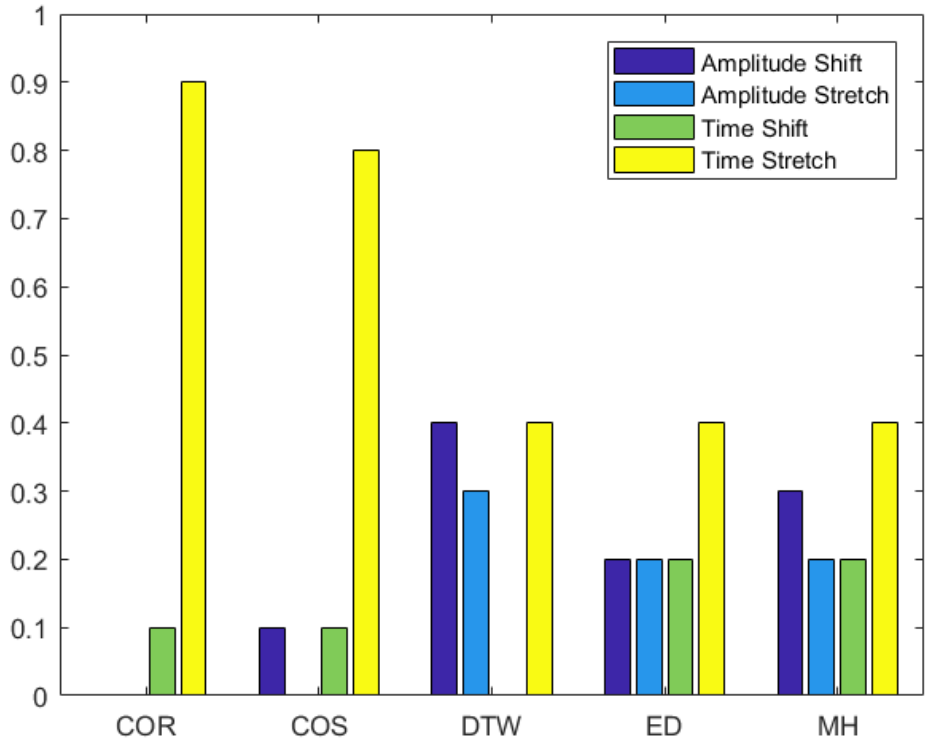

Figure 3.2: Comparison of similarity measures

warping has negligible error with time shift. These results provide an example of what can be expected when they are used with simulation or PMU time series data.

3.3 System Level Experiment Methodology

The system level experiment is setup to determine whether system response error can determine the total system accuracy. This addresses the question: is it possible to determine if any models or the approximate percentage of models in the system are inaccurate and need to be updated, with out needing to test at each individual bus? This is determined by calculating the correlation between system accuracy, as defined in Equation 3.1, and system response error described below.

This experiment is performed within the RTS96 test system [47, 48], using Siemens PSS/E software. Fourteen CLMs are randomly placed on loads in the system enhancing the RTS96 case to create a load model benchmark system. The remaining 37 loads are modeled with the static ZIP load model. Test systems are generated by replacing some ZIP load models from the benchmark system with CLM in the test system and some CLM in the benchmark system to ZIP load models in the test system. Switching load models creates "inaccurate" and "accurate" load models as a method to change the accuracy of the system. The "inaccurate" load models are those in the test system that are different from the benchmark system. The buses with the same load models in the test system and benchmark system are "accurate" load models. Switching these load models will also create difference responses, as described in Section I.

A hundred of benchmark and test systems are created using the randomized placement of CLMs, based on a uniform random distribution, to reduce the sensitivity of the results to location of the CLM in the system. The percentage of buses in the test system with accurate load models is called the system accuracy. System accuracy is defined in Equation 3.1 and is also used in the Bus Level Experiment.

$$\text{accuracy}_{\text{system}} = \frac{\text{Buses with accurate load models}}{\text{total number of buses with loads}} \tag{3.1}$$

An example benchmark and test system pair at 50% system accuracy will have half of the CLMs removed from the benchmark system. The removed CLMs will be replaced with ZIP load models. System accuracy quantifies how many dynamic load models in the system are accurate. Accurate dynamic load models in the test systems are those models which are the same as those in the benchmark system.

A bus fault is used to create a dynamic response in the system. Over a hundred simulations are performed where the location of the fault is randomized to reduce the sensitivity of fault location in comparison to CLM location. The bus fault is performed by applying a three-phase to ground fault with a duration of 0.1 s. During this fault, there is an impedance change at the bus fault causing the voltage to drop at the bus and a change in power flows throughout the system. The fault is cleared 0.1 seconds after it is created, and the power flows returns to a steady-state.

The output captured from the simulations are voltage magnitude, voltage angle, and frequency from all of the load buses, and line flow active power and reactive power. The

output from the benchmark system is compared to the test systems using the similarity measures outlined in Section 3.2. The response error generated by DTW, cosine distance, and correlation coefficient are a single measure for the entire time span of each output at each bus. The response error from Manhattan and Euclidean distance is generated at every time step in the time span. The error at each time step is then summed across the time span to create a single response error similar to the other similarity measures. The generation of response error for Manhattan and Euclidean distance is shown by Equation 3.2.

$$\text{error}_{\text{response}} = \sum_{t=1}^{T} s[t] \tag{3.2}$$

Similar to response error, system response error is calculated from the difference between the output of buses between the benchmark and test systems. However, system response error is a single metric which is the sum of all the response errors from each bus.

Three time spans are tested: 3 seconds, 10 seconds, and 30 seconds. The disturbance occurs at 0.1 seconds and cleared at 0.2 seconds for all the scenarios. These time spans are chosen to test the sensitivity to the transient event occurring in the first 3 seconds, and sensitivity to the dynamic responses out to 30 seconds.

The Pearson correlation coefficient is calculated between system accuracy and system response error using the student t-test, to determine the relationship between the two. The student t-test is a statistical test to determine if two groups of results being compared have means which are statistically different. The output of the Pearson correlation coefficient is the r and p-value. The r-value denotes the direction and strength of the relationship. R-values range from -1 to 1, where -1 to -0.5 signifies a strong negative relationship and 0.5 to 1 signifies a strong positive relationship between the groups. For this experiment, a strong negative relationship implies that as the system accuracy increases the system response error decreases. This is the relationship typically assumed by those performing measurement-based techniques. The p-value is the value which determines if the two results are different. A p-value of less than 0.05 signifies a statistically significant difference between the two groups of results being compared. Therefore, a p-value less than 0.05 signifies a statistically significant relationship quantified by the r-value.

3.4 System Level Experiment Results

In this section, the correlation between response and system accuracy is calculated to evaluate the ability of various time spans, output types, and similarity measures to predict system accuracy as used in measurement-based techniques.

An example outputs from these results is visualized in Figures 3.3 and 3.4. The plots compare the reactive power times series data from a bus in the benchmark system and test systems at two levels of system accuracy in a system undergoing a bus fault at the same bus. Figure 3.4 shows the benchmark and test system responses with low system accuracy, 8%. Figure 3.3 shows the responses with high system accuracy, 92%.

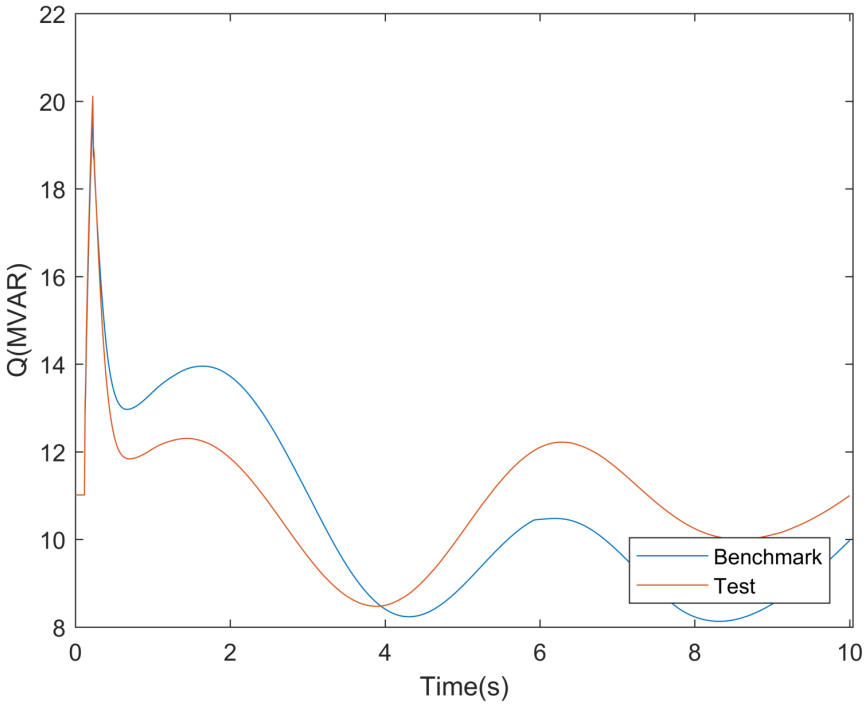

Figure 3.3: Reactive Power Time Series Plot of Low System Accuracy and High Response Error with Generator Outage

The response from the high system accuracy test system has a better curve fit to the benchmark system than the low system accuracy test system. This visual comparison confirms that with an appropriate similarity measure the response error should decrease

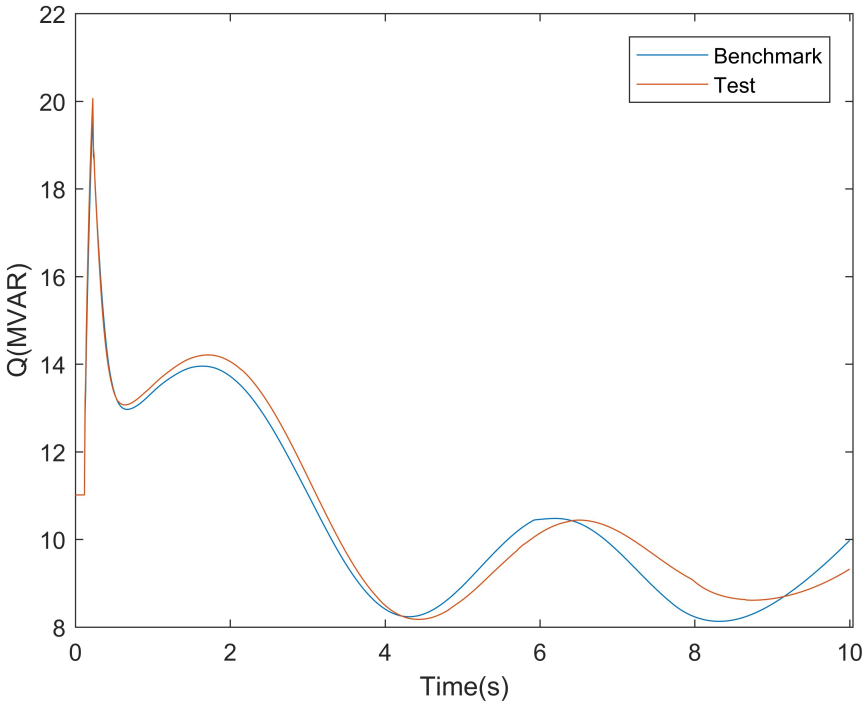

Figure 3.4: Reactive Power Time Series Plot of High System Accuracy and Low Response Error with Generator Outage

as system accuracy increases.

The results from all the simulations determining correlation between system accuracy and response error as grouped by the metrics used are shown as r-values in Figure 3.5. R-values of less than -0.5 are highlighted in orange to show they represent a strong relationship. R-values greater than -0.5, which do not have a strong relationship, are in white. All resulting p-values are found to be lower than 0.05, meaning all r-value relationships are statistically significant. The similarity measures listed in the plots use the same abbreviations as in Figure 3.2. The output types listed in the plots are abbreviated with: voltage angle (ANG), voltage magnitude (V), frequency (F), line active power flow (P), and line reactive power flow (Q).

Out of the 75 combinations of metrics tested in this experiment, only 12% yielded statistically significant differences. Considering the visual verification that indeed response error should decrease as system accuracy increases from Figures 3.3 and 3.4, the

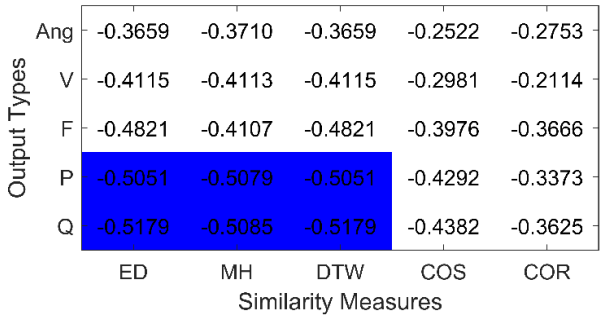

(a) 3 second time span

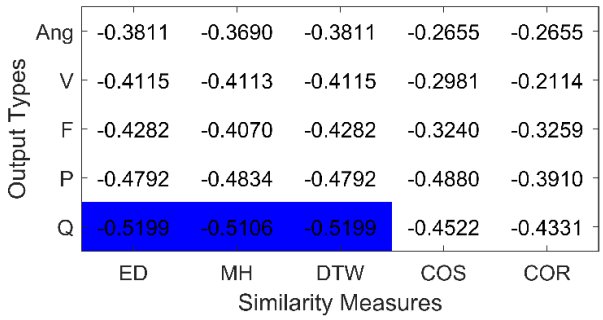

(b) 10 second time span

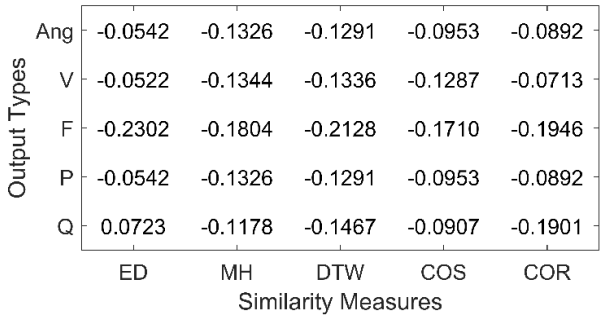

(c) 30 second time span

Figure 3.5: Bus fault R-values for system level experiment for time spans: a) 3 seconds, b) 10 seconds, c) 30 seconds

lack of strong negative correlations seen in Figure 3.5 are concerning. Only the three and ten-second time span simulations have strong correlation relationships, none of the

thirty-second scenarios have strong relationships. During a thirty-second simulation, the last ten to thirty seconds of the output response will flatten to a steady-state value. Therefore, in a thirty-second simulation there are many error data points that might contain flat steady-state responses limiting curve fitting opportunities and reducing a correlation relationship. This can explain why none of the thirty-second scenarios have strong relationships.

The distribution of the r-values from the overall strongest correlation relationship, with an r-value of -0.5199, is examined to further investigate the correlation results. Figure 3.6 visualizes the distribution of the response error for this r-value at the tested levels of system accuracy.

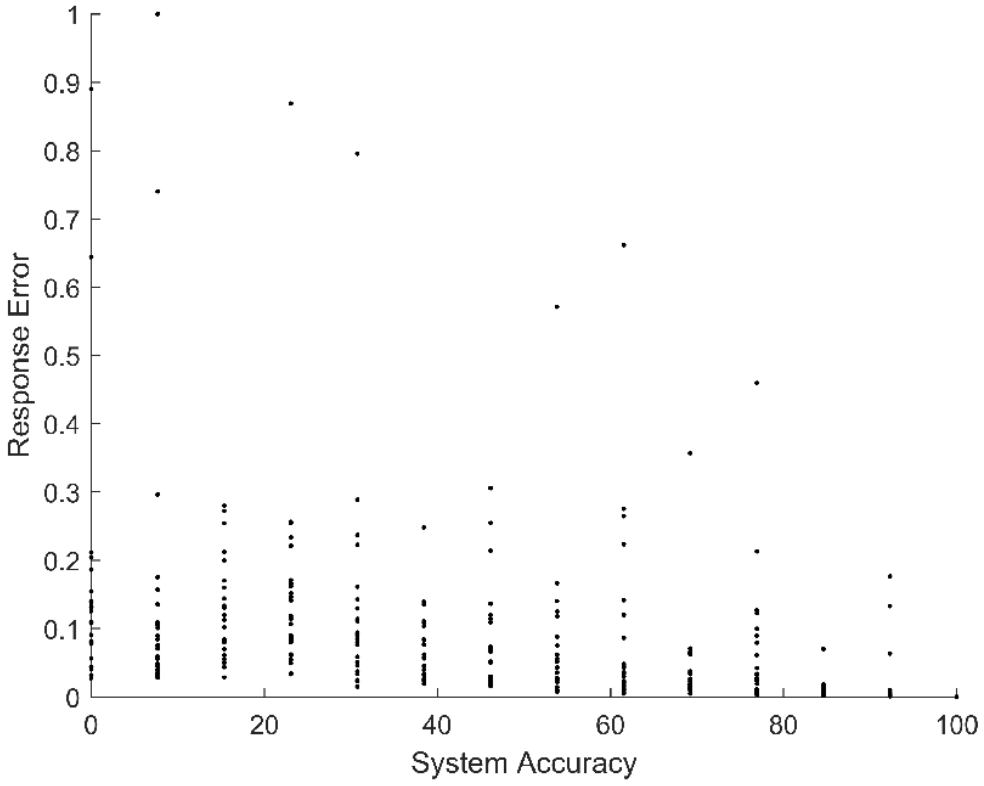

Figure 3.6: R-value distribution

The response error in figure 3.6 is normalized for a clearer comparison. A general

negative correlation is seen, where there is lower response error at higher system accuracy. However, there are several outliers in the data preventing a stronger overall correlation, particularly between system accuracy levels 0% and 70%. This suggests at lower system accuracy levels the correlation is not as high as in the overall distribution. To test this, the correlation between system accuracy ranges is calculated to highlight where the weakest correlation regions exist. Table 3.3 outlines the correlation at the following system accuracy ranges.

Table 3.3: Correlation within system accuracy ranges

0-30%	38%-54%	62%-77%	84%-100%
-0.0632	-0.2964	0.0322	-0.4505

Seen in Table 3.3, the correlation is greatly degraded at the low levels of the system accuracy ranges, even reversing the r-value relationship from negative to positive between levels 62% and 77%. An ideal scenario would have a constant strong negative correlation through all system accuracy levels. This highlights a potential low effectiveness of measurement-based techniques using these testing conditions at low system accuracy levels. Overall, the results from this experiment highlight the lack of correlation between response error and system accuracy across all metrics.

The application of the system level experiment is to use any of the metrics combinations that showed strong negative relationships in a measurement-based optimization program. Such an optimization program could change the dynamic load models in the system to reduce system response error in order to improve system accuracy. However, in order for such an optimization program to successfully improve system accuracy, there needs to be a strong negative correlation between system accuracy and system response error. Additionally, even with an overall strong negative correlation, Table 3.3 shows that such an optimization program may determine a local minimum at a lower accuracy level to be the global minimum due to the lower correlation relationship strength found at lower accuracy levels.

These results identify the need for measurement-based techniques, and potentially other power systems time series data curve fitting techniques, to evaluate the assumption that the system response error is correlated to the system accuracy. It cannot be assumed

measurement-based techniques using similarity measures yield meaningful results. Any optimization or other estimation technique using the reduction of system response error will not yield accurate results of findings without a strong correlation between system response error and system accuracy.

3.5 Bus Level Experiment Methodology

The bus level experiment is setup to determine whether response error from an individual load bus can indicate if a load model being used at the bus is accurate. In comparison to the system level experiment which looked at system wide model accuracy, this experiment looks at model accuracy at the bus level. The results of this experiment are the p-values from the student t-test, indicating whether there is a statistical difference between the response error from buses with accurate and inaccurate load models. The p-value is the value which determines if the two results are different. A p-value of less than 0.05 signifies a statistically significant difference between the two groups of results being compared.

The same system and system setup are used in this experiment as in the system level experiment. This experiment excludes comparing the output from line flow active power and reactive power with the previously used outputs of frequency, voltage angle, and voltage magnitude of the buses. In this experiment the simulations are performed at various levels of system accuracy to reduce the sensitivity of the results to the system accuracy. By reducing the sensitivity of the results to fault placement and system accuracy, the results focus the correlation to between response error and load model accuracy. All other metrics remain the same as the system level experiment.

The response error from all the simulations are compared by output type, time span, and similarity measure, and binned into groups of buses with accurate load models and buses with inaccurate load models. A t-test is performed on the binned response error to determine if there is a statistically significant difference between the error from buses with accurate load models and buses with inaccurate load models. The results of this experiment are the p-values from the response error separated by disturbance scenario, output type, time span, and similarity measure.

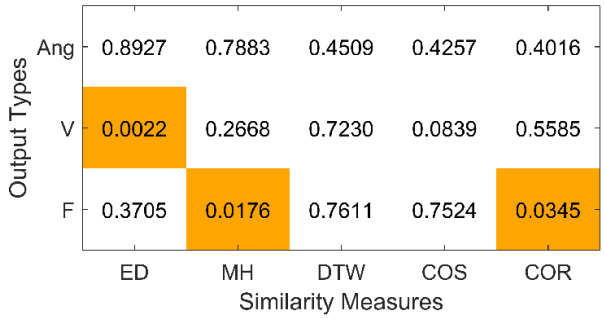

(a) 3 second time span

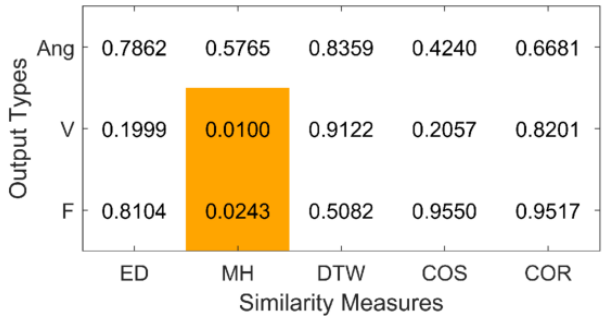

(b) 10 second time span

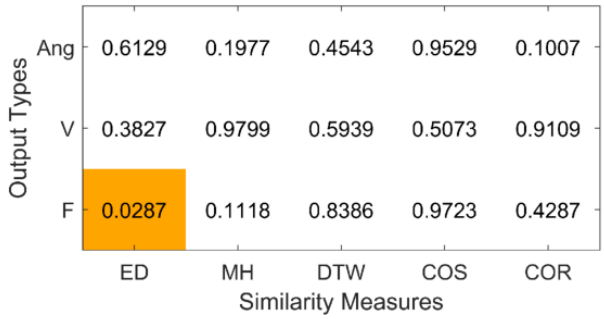

(c) 30 second time span

Figure 3.7: Bus fault P-values for bus level experiment for time spans: a) 3 seconds, b) 10 seconds, c) 30 seconds

3.6 Bus Level Experiment Results

The bus level experiment tests whether there is a statistical difference between the response error at individual buses with the accuracy of the load models at the buses. The p-values are calculated using response error from the output types, time spans, and similarity measures. Figure 3.7 shows these p-values.

Less than 15% of the combinations of time span, output type, and similarity measure have significant p-values. It is noted that the combinations of metrics best used for this experimental setup are different than those in the system level experiment. This experiment highlights a serious concern for other experiments using measurement-based techniques. Only select combinations of metrics in this experiment yielded significant differences, and this same result is likely present with other measurement-based experiments whether they involve changing load models, changing load model parameters, or changes in other dynamic models.

The direct application of this experiment is to use any of the disturbance type, output type, time span, and similarity measure combinations that showed significant p-values in a measurement-based machine learning technique to identify if a bus in the system need a load model updated or a different load model. There needs to be a significant difference between response errors from buses with poor fitting or inaccurate load models and those which are accurate for such a machine learning algorithms to give meaningful results, whether it be from simulation or PMU outputs. In this case, if the machine learning algorithm was using a combination of metrics that did not have a proven significant difference between response error from buses with inaccurate and accurate load models, the machine learning algorithm would be unable to accurately tell the difference between the groups, causing the results to be inaccurate.

The results from this experiment confirm the same conclusion from the system level experiment that there needs to be verification testing showing that the chosen measurement-based metrics used to calculate error will capture true differences between incorrect models and correct models. It cannot be assumed that any combination of metrics used in measurement-based techniques will yield meaningful results.

3.7 Conclusion

This paper investigates common metrics used in measurement-based dynamic load modeling techniques to generate response error. These metrics include similarity measures, output types, and simulation time spans. The correlation between response error and accuracy is evaluated by comparing the system accuracy to system response error with the system level experiment and load model accuracy to bus response error with the bus level experiment. Both experiments demonstrated there is a lack of combinations of metrics that deliver significant findings. It is noted that the combinations of metrics best used in the bus level experiment are different than those in the system level experiment. This same result is likely to be found with other measurement-based experiments whether they involve changing load models, changing load model parameters, or changes in other dynamic models. These experiments expose a significant concern for measurement-based technique validity. This study raises awareness of the importance of careful selection and validation of similarity measures and response output metrics used, noting that naive or untested selection of metrics can deliver inaccurate and meaningless results.

These results implicate that optimization or machine learning algorithms that use measurement-based techniques without validating their metrics to ensure correlation between error and accuracy may not generate accurate or meaningful results. These methods to determine the effectiveness of the use of these common metrics are specific to these experiments of model accuracy. Future work can expand these methods to dynamic model parameter tuning experiments.

Chapter 4: Transient Voltage Stability Effects on Hosting Capacity of Behind-the-Meter Devices

4.1 Introduction

The contribution of distributed energy resources (DER) is broadening across the U.S., with U.S. market penetration forecast to increase from 4.7% in 2015 to 6.7% in 2040 [49]. The presence of large amounts of DERs can cause challenges in forecasting uncertainties in both day ahead markets and long term planning, coordination of control between several time scales spanning from operations to markets, and grid stability [50–52]. Hosting capacity methods have been developed as a way to determine the maximum amount of DERs a network can integrate without causing stability concerns such as those mentioned in [51]. These hosting capacity methods are typically performed using PV curves to evaluate voltage stability or evaluate based on transient voltage stability [53–56].

Opportunities have been identified for DERs, and large scale inverter-based resources, to provide voltage and frequency regulation through proper implementation of reactive power support controls [57, 58] and inertia emulation and frequency response controls [59, 60]. For these applications it is necessary to evaluate the transient stability effects of DERs because voltage and frequency regulation controls respond on the order of sub-seconds to seconds depending on the application. Therefore, it is also necessary for hosting capacity studies to evaluate the transient voltage stability. Similar to hosting capacity studies, risk evaluations have been developed that do assess the transient stability [61, 62]. These risk evaluations provide the user the information to determine an acceptable amount of DERs or variable energy generation to allow on the system according to a calculated risk associated with the variability of the resource and the probability of contingencies on the system. Another benefit of the method developed by [61] is the consideration of multiple resource variability. As multiple resources in a system can be variable, such as PV solar and wind generation being variable but with separate variabilities, it is an important to consider the effects from multiple variabilities in risk or hosting capacity studies. An additional variable element of the electrical

grid, which has not been considered in mentioned risk or hosting capacity works, is the variability of load dynamics.

Many DERs are installed at industrial and commercial facilities as methods to reduce electricity costs and reduce their carbon footprint. Industrial and commercial facilities have diverse dynamic load compositions including fans, pumps, other industrial motors. The transient stability effects of certain dynamic load compositions have been well studied, such as induction motors degrading transient voltage stability [63–65]. Additionally, induction motor loads have been shown to reduce stable penetration level of wind generation in distribution networks [66]. DERs and dynamic loads are interlinked in both placement and transient stability, therefore their interaction and variability must be evaluated in hosting capacity studies.

This paper evaluates the transient voltage stability effects from all dynamic behind-the-meter devices including DERs and dynamic loads. Argument is made for the the necessity of considering the combined effects of these devices on transient voltage stability and how these effects can impact hosting capacity. These results point to how these combined effects need to be evaluated to identify vulnerabilities in systems due to all behind-the-meter dynamic behavior. The methods deployed to evaluate these effects can also be used to evaluate the effectiveness of measures such as voltage and frequency regulation controls to increase the hosting capacity of DERs. The main contributions of this paper are: 1) demonstrate the need for assessment of all behind-the-meter dynamics and 2) suggest methods to determine the hosting capacity of all behind-the-meter devices that includes the transient voltage stability.

4.2 Behind-the-Meter Effects on Transient Stability

The dynamics from DERs originate from their controls to activate tripping to provide auxiliary grid services such as voltage and frequency support. Without these controls DERs would behave as a constant negative load from a bulk power perspective. With these controls negative transient stability effects can be caused, such as large amounts of DERs tripping at once causing a sudden change in generation. Events such as this have occurred in California resulting in 900 MW of solar being tripped due to over-voltage transients in 2017 [67]. These types of events precipitated the requirements of fault ride through capabilities of DERs in the update of California's Rule 21 [68]. With the

advent of the updates to Rule 21, DERs can also provide auxiliary services to benefit the transient stability of the grid, such as voltage and frequency support with dynamic volt-var management. Due to these capabilities the transient stability effects from DERs must be considered in reliability, risk, and hosting capacity studies.

The effects of dynamic loads on transient stability of the grid, especially on transient voltage stability with large industrial loads consisting of induction motors have been heavily studied as mentioned. To address the concerns of transient stability effects from dynamic loads, the Western Electricity Coordinating Council put efforts into the development of the composite load model [69]. The composite load model consists of four types of motor loads, a power electronic load, and static loads consisting of constant impedance, constant current, and constant power. This model was designed to assist utilities improve their load modeling accuracy in transient stability studies. However, parameter estimation of dynamic load models based on historical or real-time utility data such as phasor measurement units (PMUs), a method know as measurement-based estimation, remains a challenge [37, 41, 70]. The Load Model Data tool developed by the Pacific Northwest National Laboratory assists with dynamic load model parameter identification with taking a component based approach, basing model parameters on season, geographical location, and general load type (industrial, commercial, agricultural, residential) among others [71]. With this ability to adequately represent dynamic load behavior it is important to study their effects on transient stability in all relevant studies, such as reliability, risk, and hosting capacity.

4.3 Transient Voltage Stability Study of Behind-the-Meter Devices

4.3.1 Methods

The study examines the effects from varying penetrations of DERs and dynamic load compositions on transient voltage stability and how this can change the hosting capacity of behind-the-meter devices. The transient voltage is studied using a 12 bus system simulated in PowerWorld using the distributed energy resource model, DER_A, and dynamic composite load model, CMPLDW. The load components of the composite load model are: Motor A (constant torque loads such as commercial AC and refrigerators), Motor B (high inertia loads such as fans), Motor C (low inertia loads such as pumps), Motor D

(single-phase residential air conditioners), power electronics, constant impedance, constant current, and constant power. Motor D is not considered in this study due to the single-phase and seasonal nature of this load. In systems with considerable single-phase residential air conditioners the effects of this type of load should be studied. The variation of DER active power generation is considered in this study, with the omission of reactive power generation as most DERs are installed for their active power contributions.

A line fault on the line connecting Bus 4 and 5 is simulated in the system to demonstrate the effects of these behind-the-meter dynamics on the transient voltage stability. The line fault occurs at 1 second followed by both ends of the line opening 5 cycles after the fault.

4.3.2 Individual Device Effects

First, each device is varied individually to examine the isolated voltage stability effects due to each device. The DER active power generation amount at each load is set to a percentage of the total load. The DER percentage is varied from 0% to 100% at 2.5% increments. The voltage output at each of the buses in the system is collected to determine the minimum and maximum of the transient voltage swings across all of the buses due to the simulated line fault. Examples of the time series output is seen in Figure 4.1, where (a) shows the results from the DER percentage of 52.5% of the load and (b) shows the results from the DER percentage of 82.5% of the load.

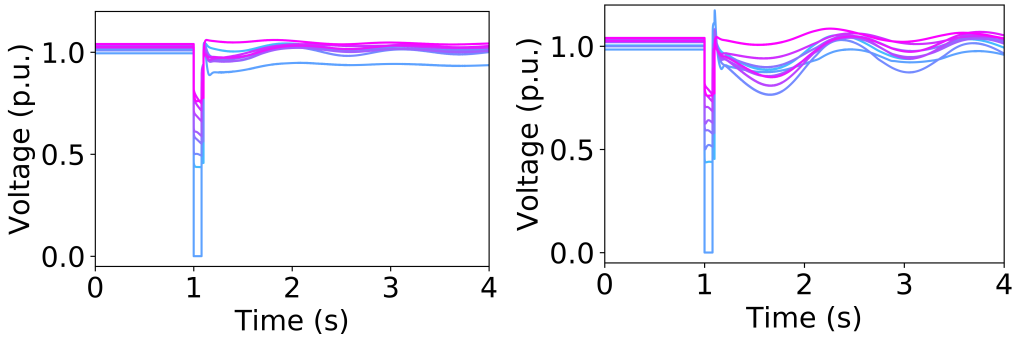

(a) 52.5% DER (b) 82.5% DER

Figure 4.1: Time series voltage from each bus during line fault with DER percentage of a) 52.5% and b) 82.5% of the load.

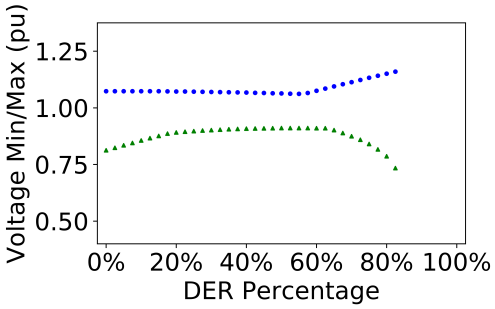

Figure 4.2: Minimum and maximum voltage swing values from varying contributions of DER as a percentage of load.

The minimum and maximum voltage values are collected from the time series output after the line is opened. The examples shown in Figure 4.1, simulated at 52.5% and 82.5%, also contain the highest and lowest minimum voltage swing values respectively out of all variations of DER percentage.

The resulting minimum and maximum voltage swing values for all variations of DER percentage are shown in Figure 4.2. The simulations that were unstable due to runaway rotor angle are not plotted. As seen in Figure 4.2, this instability occurs when the DER percentage is greater than 85% of the load. These results show that the presence of DERs contributes to the stability of the system due to the ability for DERs to serve load locally. An increase of DER contribution from 0% to 52.5% of total load increases the minimum voltage swing from 0.81 pu to 0.91 pu. However, as the mismatch between load and generation becomes too great, around the DER percent of 80%, the system becomes unstable.

The effects from the dynamic load types are evaluated the same way. When the dynamic load component percentage of total dynamic load are varied, the other portion of the dynamic load is taken to be constant power load. The resulting minimum and maximum of the voltage swings across all of the buses at varying dynamic load component percentages are illustrated in Figure 4.3. Dynamic load types do not have as great an effect on voltage stability as DER contribution when considering a contribution ranging from 0% to 100%. However, when considering a range from 0% 50%, a more realistic DER operating range and dynamic load percentage for each type, the minimum voltage swings have approximately the same range of variation with around a ± 0.1 pu change. A change of 0.1 pu in voltage could make the difference in whether protection relays trip,

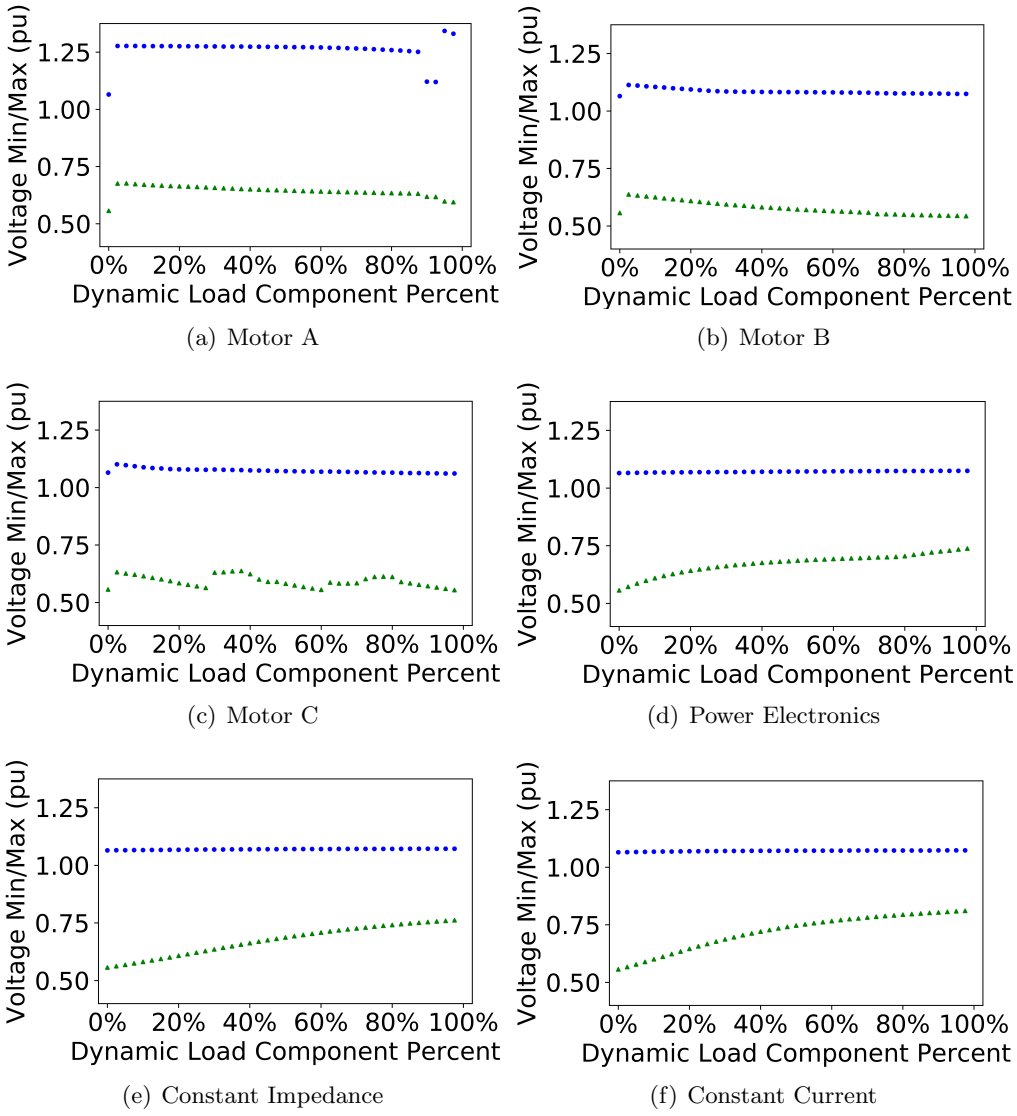

(a) Motor A

(b) Motor B

(c) Motor C

(d) Power Electronics

(e) Constant Impedance

(f) Constant Current

Figure 4.3: Minimum and maximum voltage swing values from varying percentages of dynamic load types.

resulting in a potentially more detrimental contingency. This highlights the importance of considering both DERs and dynamic loads for their transient voltage stability effects.

Examining the difference in voltage effects due to dynamic load types, similar trends are seen across motors A-C, as all are induction motors with varying inertia and torque.

Also, similar trends are seen across power electronics, constant impedance, and constant current. These loads also have similar behaviors due to their load being calculated on different exponential values of voltage. These two grouping of behaviors are here grouped in two classes, the motor load class and the static load class. The shift from all constant power load to all motor load has an immediate increase in the entire voltage profile. Constant power loads consume the same amount of power regardless of voltage, which results in the greatest load demand during transients in comparison to other static loads. This behavior is the cause for why the minimum voltages across all static load types increase as the percentage of that component increases and constant power load decreases. Induction motors draw more current when the voltage drops due to a transient event, causing increased voltage instability. At full induction motor load the minimum voltage swing values are as low as just as low as full constant power load. However, a combination of both constant power and induction motor results in an improved minimum voltage.

4.3.3 Combination of Device Effects

Next it is important to consider how the contribution and interaction of both the DERs and dynamic load types will create a combined effect on the transient voltage stability. To consider this, the variation of each of the dynamic load components is varied against a variation of DER active power generation. As the maximum voltage swing values had little change from individual device variation, they are not considered in this section. The minimum voltage swing values are determined using the same method in the previous section. The results are shown in Figure 4.4.

The combined effects of DERs and each dynamic load type follows a predictable and smooth gradient across the solution space when compared to their individual effects. However, there is a combined effect due to both making it necessary to understand and consider the effects of the DER contribution and dynamic load composition. When DER controls or more sensitive trip settings are activated on DERs or loads the gradients might not be as smooth or predictable.

Next we investigate the effects due to numerous dynamic load types with DERs. There is an exponential relationship between number of variable devices and simulations to perform, making it computationally expensive to consider all dynamic load type

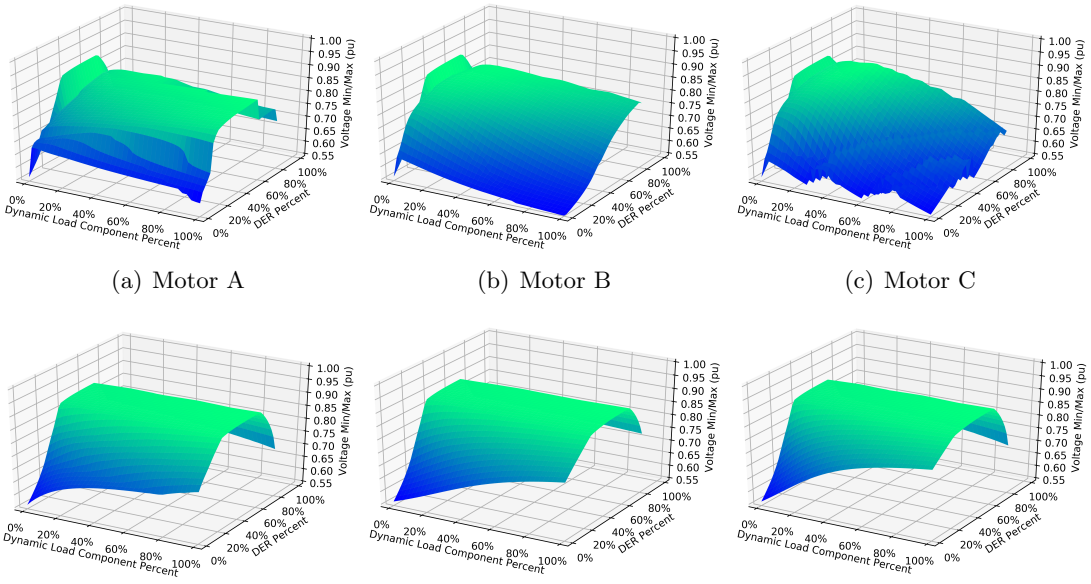

(a) Motor A (b) Motor B (c) Motor C

(d) Power Electronics (e) Constant Impedance (f) Constant Current

Figure 4.4: Minimum voltage swing values cross variations of DER percentage and dynamic load types percentage.

variations together. Instead, we consider one dynamic model type from the motor load class, Motor A, and one from the static load class, constant current, with the addition of constant power load, as constant power load was considered in the combined variations just examined.

The effects of these behind-the-meter devices on the minimum voltage swing values are visualized in Figure 4.5. A uniformly distributed sampling of percentage of each device was used to sample the solution space with simultaneous variations in all the devices. Approximately 8,000 multivariate data points were produced from this sampling. The boxplots demonstrate the effects on minimum voltage swing values from cross variations between devices, where each plot shows the range of voltage values found per percentage band of device across all variable percentages of all other devices. The blue dots show the original effects from the individual devices. There are not individual effects to report for constant power, as this load types filled the other percentage of the load when the effects from individual load types were calculated.

The results demonstrate the trends from multi variable devices (boxplots) are similar

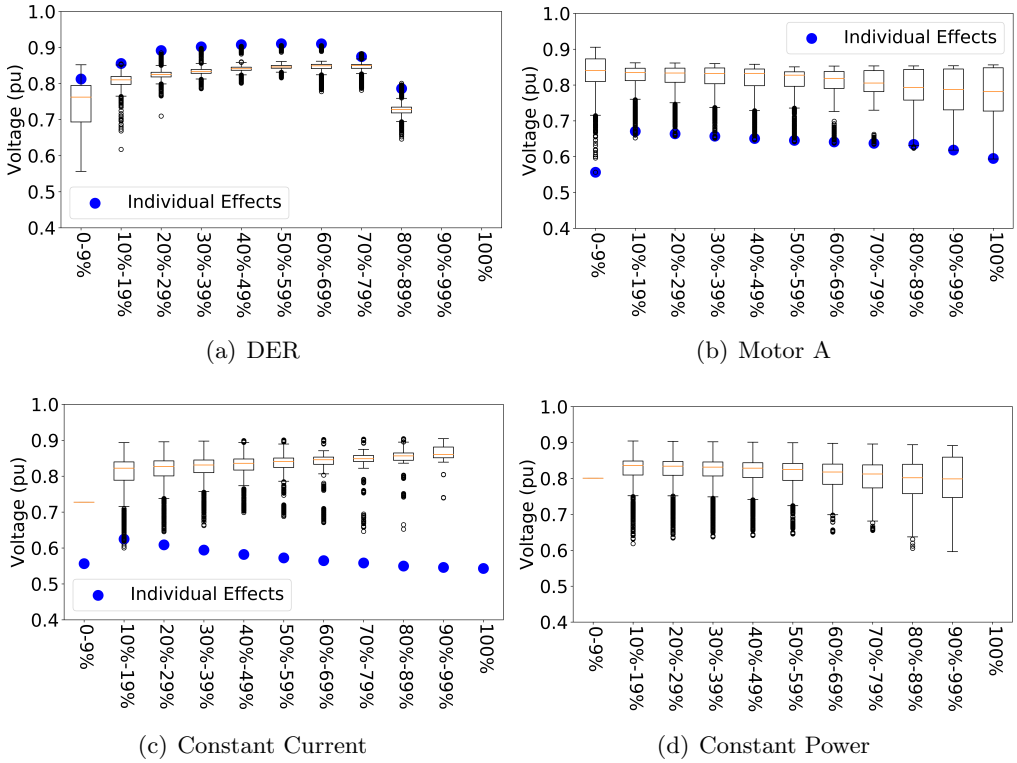

(a) DER (b) Motor A

(c) Constant Current (d) Constant Power

Figure 4.5: Minimum voltage swing values from all cross variations of DER and dynamic load types: motor A, constant current and constant power. Each box shows the results from all minimum voltage swings across all variations of all other devices for the percentage band specified of the selected device.

to those seen in the original individual variations of devices (blue dots). Due to the inclusion of the dynamic load types the minimum voltage swing values from all variations of DER are reduced. This signifies that the inclusion of dynamic loads in the system degrades the transient voltage stability, and therefore if hosting capacity is based on minimum voltage swing the hosting capacity would also be reduced. On the other hand, when a system has dynamic loads, the inclusion of DERs can improve the transient voltage stability of the system, as seen by increased minimum voltage swing values from the individual effects to those in the boxes.

These results can be used to form an understanding of what the hosting capacity of each device, or combination of all devices, should be for the system. The hosting capacity could be evaluated by setting a minimum voltage swing limit and determining

the capacity by the percentages of each device that are above that minimum voltage swing limit. In this study, if we were to determine the hosting capacity on a limit of 0.65 pu, then to remain within the limit the hosting capacity of DERs would range from 20% to 80% of the total load. To note, in this study only one contingency was used to evaluate stability. A more realistic evaluation of transient voltage stability would include $N-1$ or $N-2$ contingencies. Additionally, the transient voltage stability could be evaluated using different values other than minimum voltage swing to determine if the system is stable, as most low voltage relay settings have delay times to recheck the voltage value. Therefore, sustained low voltage or steady state voltage after the contingency could be used to evaluate transient voltage stability. However, with the onset of controls and devices that are capable of activating or tripping devices during transients it is necessary to perform transient stability simulations to capture the effects of these controls and possible trips even if the value used to evaluate hosting capacity is not taken within the transient time frame.

4.4 Conclusion

This paper studies the effect of behind-the-meter devices on the transient voltage stability of the system. The effects from varying the penetration of DERs and dynamic load types within the composite load model are evaluated as both individual effects and combined effects. The results demonstrate the need to consider the transient voltage stability effects from all of these devices as their individual and combined effects change the minimum voltage swing values seen within the system. If the hosting capacity is determined from these swing values or other voltage values, the hosting capacity of DERs or dynamic loads will change based on the inclusion of these devices. The addition of dynamic loads to the studied system containing DERs reduces the minimum voltage swings which reduces the hosting capacity based on transient voltage stability. However, the addition of DERs to the system containing dynamic loads improves the transient voltage stability of the system. Future work to expand the applications of this study include evaluating: DER controls for voltage and frequency support, DER and dynamic load placement in the system, system architecture, N-1 or N-2 contingencies, and optimization methods to identify solutions close to limits used to determine hosting capacity.

Acknowledgment

This research was completed by Idaho National Laboratory with funding from the U.S. Department of Energy Wind Energy Technologies Office. Idaho National Laboratory is operated by Battelle Energy Alliance under contract No. DE AC07-05ID14517 as part of the Microgrids, Infrastructure Resilience and Advanced Controls Launchpad (MIRACL) project.

Chapter 5: Transmission Hosting Capacity of Distributed Energy Resources

5.1 Introduction

The increasing generation contribution of distributed energy resources (DERs) has created challenges on both the distribution and transmission grid. It is important to characterize these impacts to be able to predict and prevent instabilities and reductions in reliability on the electrical grid. Also to create adequate practices and planning methodologies that enable DERs' continued growth.

Currently, DERs are a salient part of power system planning with the U.S. market penetration forecasted to increase from 4.7% in 2015 to 6.7% in 2040 [49]. Numerous factors drive this increase, including: environmental drivers such as limiting green house gas emissions and avoidance of new transmission and generation construction [72–75], or national/regulatory drivers such as energy security through diversification [72]. The impacts of high DER contribution on the distribution grid have been heavily studied and numerous optimal placement and sizing methods–as well as hosting capacity methods–have been developed to avoid negative technical impacts while maximizing DER penetration. The technical impacts include overvoltage, power harmonic distortion, thermal overloading of equipment, exceeding equipment short circuit capacity, and maloperation of protection equipment [76, 77]. Hosting capacity (HC) methods determine the maximum amount of DERs that can be integrated into the power system while maintaining the required system performance, such as the technical impacts just mentioned. Optimal placement and sizing methodologies aim to increase HC through leveraging topology and system connectivity properties.

A key component of the HC and optimal placement and sizing methods is the inclusion of uncertainty in the system and DERs. The uncertainty is accounted for with either probabilistic or both probabilistic and deterministic strategies, often completed with Monte Carlo assessments. In [78–80], Monte Carlo based methods are used to assess the impact of either distributed generation (DG) placement and size uncertainty, load

or generation uncertainty, or network topology variability in overall HC of DGs. These studies constrain the HC via technical and economic limits. These studies highlight the importance and need to include uncertainty assessments or at a minimum deterministic variations when evaluating HC. They also all solely evaluate steady state technical constraints and do not consider transient stability limits.

Transient stability is an important consideration, especially in light of new regulations in the U.S.A. allowing DERs to participate in ancillary service markets of the transmission grid [81]. The type and operating strategies of distributed wind generators can improve the reactive power savings and impact steady state and transient voltage stability as shown in [82]. In [83], the dynamic and steady state voltage stability is evaluated under a moving cloud scenario with solar PV. This demonstrates how the dynamic characteristics can be more limiting than the static snapshots, highlighting the importance of dynamic and transient stability on HC.

Another consideration and variability in HC is load types models, which can be modeled as either dynamic or steady state. In [84, 85], voltage dependent load models are considered with DER placement and sizing, demonstrating how load composition impacts optimal DER portfolios. The effect of time-varying load models and solar PV size and placement is studied in [86]. HC of solar PV in the distribution grid is compared between distribution systems with residential, industrial, commercial, and a mix of time-varying load types. This work demonstrates how the variation in the hourly load profiles impacts the solar PV HC, with the smallest HC found with residential systems which have the greatest mismatch in solar PV generation and load demand throughout the day. [87] also notes the importance of considering different periods of time and the lack of HC studies that address this, while introducing a dynamic HC study that considers hourly time frames on numerous days. These studies highlight the effects of load models, however none included dynamic load models in transient stability simulations.

The impacts of DERs in the transmission systems have been less studied than in the distribution system. Impacts on transmission transient stability have been noted due to high DER contributions in [37, 54]. Transmission expansion planning studies have identified significant impacts on their analysis due to the introduction of DERs [88–94]. These techno-economical transmission planning methods have been developed in a similar vein to distribution system DER HC studies to ensure stable and cost effective planning for higher DER contributions on the transmission grid. However,

studies directly determining HC of DERs in the transmission grid are limited. A need has been identified for development of transmission grid DER HC methods, [54] studies the impacts of increasing DG penetration on the transient stability of a transmission system. The results show the $N-1$ line loss transient impacts of increasing DER penetration, with various types of DG such as asynchronous and synchronous machines and power electronics. The findings suggest that contributions of DG in the transmission system can improve the transient stability by reducing large power flows, which detrimentally affect the damping of oscillations in the system. This work describes how the contribution of DERs can improve transient stability in transmission systems, which provides additional argument for encouraging the growth of DERs. However, also similar to distribution systems, high contributions of DERs do have the potential to negatively impact both the steady state and transient stability of transmission systems and it is important to be able to identify the HC as well as other advanced metrics that provide more accurate representation of the current state of the system.

This work addresses HC of DERs in the transmission grid and evaluates the impacts and importance of different modeling strategies. There are numerous modeling setup considerations to scope when developing a DER HC method for transmission systems. These considerations include timeframe and scenarios, uncertainty, steady state and/or transient stability constraints, and scope of models to include such as dynamic load and DER transient models. It is accepted that these factors can impact the results of a HC study as shown in the literature reviewed, however the importance and magnitude of impact of these factors is not known. This study addresses the questions of the relative importance of these considerations and their impacts on HC results. The HC of DERs on the 2,000-bus synthetic grid overlaid on the Texas Interconnect [95] is evaluated using different modeling considerations. The contribution of this work is the evaluation of DER HC on transmission systems with assessment of the impacts on HC due to the following modeling considerations:

- Transient contingencies with dynamic load models, dynamic DER models, and steady state contingencies
- Dynamic load composition variation
- Impact of seasonal and loading variations

The remainder of this paper is organized as follows. Section II discusses the impacts of model fidelity on transmission HC evaluated with transient contingencies with dynamic load models and dynamic DER models and steady state contingencies. In Section III, we compare the transmission HC with seasonal and loading variations. Section IV details the impact of variation in dynamic load composition on Transmission HC. In conclusion, Section V discusses the implication of the results found in this study.

5.2 Steady State Contingencies and Transient Contingencies with Dynamic Load Model and Dynamic DER Model Impacts on Transmission HC

This study determines the HC of DERs in transmission systems using the 2,000-bus synthetic grid overlaid on the geographical footprint of Texas Interconnect [95]. This section evaluates the impacts of modeling differences using a Fall low loading seasonal scenario on the 2,000-bus system.

5.2.1 Experimental Setup

The modeling scenarios evaluated in this section are:

[label=]: Transient contingency with dynamic load models and dynamic DER models with high voltage support : Transient contingency with dynamic load models and dynamic DER models with low voltage support : Transient contingency with dynamic DER models with high voltage support and no dynamic load models : Transient contingency with dynamic DER models with low voltage support and no dynamic load models : Transient contingency with dynamic load models and no dynamic DER models : Transient contingency without dynamic DER or load models : Steady state contingency

The HC is defined as the maximum amount of DERs in the system while maintaining stability, as determined by stability limits. The stability limits include load loss, steady state and transient under and over voltage limits, under and over frequency limits, and rotor angle deviation. A set amount of limit violations are allowed per each contingency and the HC is determined when the amount of violations per contingency surpasses the

Table 5.1: Transient Limit Monitors for Determining Violations in Transient Stability Contingencies

Violation Type	Limit Value	Limit Duration (s)
Voltage Dip Load Bus	±0.25 pu	0
Voltage Dip Load Bus Duration	±0.2 pu	0.33
Voltage Dip All Bus	±0.2 pu	0.33
Voltage Dip Non-Load Bus	±0.2 pu	0
Frequency	<59.6 Hz	0.1
Rotor Angle	±90	0

allowed amount of limit violations. The amount of load loss allowed per contingency was 5% of the total load. A total of 100 individual violations were allowed per contingency. The transient contingency violations were determined with transient limit monitors as specified in Table 5.1, based on the Electric Reliability Council of Texas (ERCOT) standards. The steady state contingency violations were also determined with limit monitors, set by minimum and maximum bus voltages and overloading of branches. Similarly, 100 violations are allowed with steady state contingencies for determination of the HC.

A set of contingencies are used to evaluate the HC. A subset of critical contingencies were used instead of $N-1$ to reduce the computation time. The set of contingencies included a contingency from each of the areas in the system. The contingency chosen in each area corresponded to a line loss whose line had the highest power transfer distribution factor (PTDF) [96] linear sensitivity with power transfers between the different areas and the slack bus. The PTDF represents what percent of a transfer would appear on each transmission line. Therefore the line with the highest PTDF is one of the most critical lines if not the most critical line, depending on the engineering application. This selection method of contingencies is designed to capture the most severe contingencies that will limit the HC more drastically.

These contingencies were analyzed both as a steady state and transient contingency as specified in the modeling scenarios. The steady state contingencies calculate the power flow due to the loss of a line. The transient contingencies simulate a fault on a line at 1 second with both ends of the lines opening six cycles after the fault.

5.2.2 Load Modeling

All loads in power systems are inherently dynamic depending on the time scale. It is this timescale that determines which load models are required for accurate representation of load behavior. Daily or hourly load profiles capture the steady state load changes throughout the day. Typical load models for steady state loads are either static MW or voltage dependent [86]. These load models are used when evaluating steady state contingencies in this study. To evaluate transient contingencies the load can still be simulated with static load models, however, dynamic load models, which include static and dynamic components, are more representative of the behavior of real loads connected to the grid. These dynamic components have substantial impact on the transient voltage stability and rotor angle stability of the grid, and the importance of their inclusion when evaluating stability has been widely recognized [31, 97, 98]. Therefore, dynamic load models are included in this section when evaluating HC with transient simulations. The dynamic load model used in this study is the Western Electricity Coordinating Council (WECC) composite load model which includes models of four types of motors, power electronics, and static load. The parameters of the composite load model for each of the loads were generated with the load model data tool [71], and set to an assortment of residential, agricultural, industrial, and commercial feeders.

5.2.3 DER Modeling

DERs have typically been modeled as load reductions on the transmission system, which is accurate when considering steady state contingencies. For evaluating steady state contingencies in this study DER contributions are modeled as load reductions. When DERs are modeled as a load reduction their sensitivity to tripping during transient contingencies is not captured, which can detrimentally affect the stability of the grid. This was witnessed in California when 900 MW of rooftop solar tripped due to over-voltage transients [67]. Due to concerns from events such as this, fault ride through capabilities have been required in California [68]. This behavior will only be captured if DERs are modeled with trip settings. Additionally, with FERC order 841 states DERs can provide ancillary services such as voltage support to the grid and be compensated through ancillary markets [81]. These DER capabilities will impact stability on the

transmission grid and therefore must be represented when modeling transient simulations to accurately represent DERs. This study includes the DER_A model in PowerWorld to enable simulation of DER trip settings and voltage support [99]. The voltage support settings are created with the gain constant in the reactive power priority control loop in the model. The high voltage support setting has a gain constant of 50, and the low voltage support is modeled by setting the gain constant to zero and therefore is only based on the reference reactive power input as explained in [99].

The amount of DERs in the system is based as a percentage of the load at the load bus. In this section the percentage of DERs at each load bus is increased uniformly, meaning the percentage of DERs at each bus is the same throughout the system. In a system as geographically large as the Texas Interconnect it is unrealistic that the percentage of DERs at each load bus would be the same, as most DERs are rooftop solar PV and the dispersion of rooftop solar PV is neither likely to be present evenly throughout the system nor generating the same amount of power at the same time. However, this study considers total HC and not the likely DER generation scenario. Therefore, this section considers uniformly increasing DER percentages across the system to identify the maximum system hosting capacity.

5.2.4 Results

The HC is evaluated for the modeling scenarios specified earlier as A-G. The resulting DER HC for each of these scenarios are illustrated in Figure 5.1. The HC evaluated with steady state contingencies is significantly greater than all of the evaluations using transient contingencies. This finding confirms the earlier study result in [83] that HC evaluated with steady state conditions and contingencies will result in inflated results due to transient conditions being more limiting. To further investigate the scenarios involving transient contingencies, the load behavior at load bus 7051 is examined and the time-series results from the line fault between buses 7304 and 7059 are presented in Figure 5.2. The time-series plots are separated in scenarios that included dynamic load models (A,B,E) and those that did not include dynamic load models (C,D,F).

The time-series results are separated by those scenarios with dynamic load models and those without dynamic load models because the dynamic load model behavior dominates the behavior of the load, this is seen by comparing Figure 5.2 [a] to [b]. It is

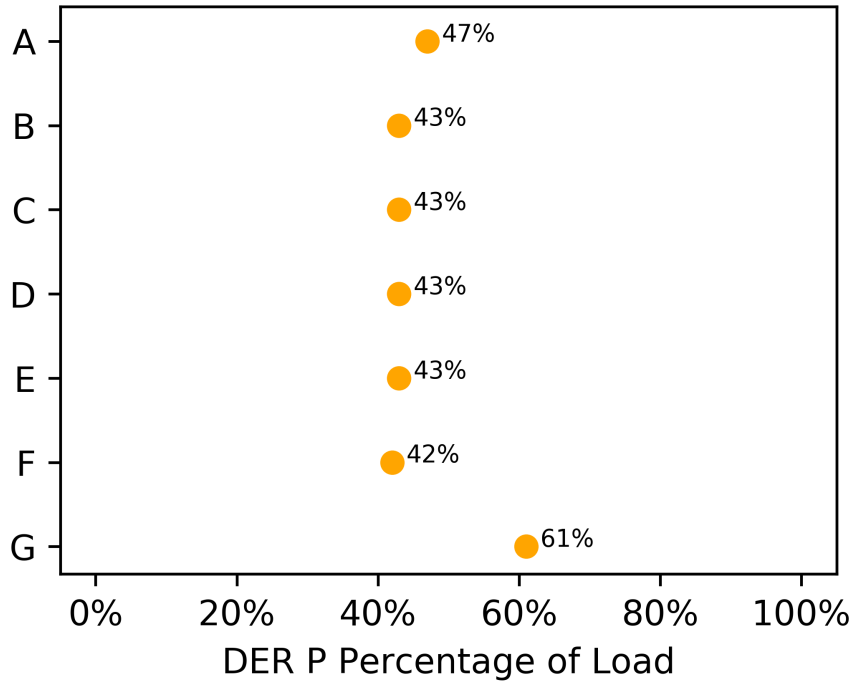

Figure 5.1: Comparison of hosting capacity of DERs on the 2000 bus synthetic grid with different modeling scenarios: A) Transient Contingency with Dynamic Load Models and Dynamic DER Models with high voltage support, B) Transient Contingency with Dynamic Load Models and Dynamic DER Models with low voltage support, C) Transient Contingency with Dynamic DER Models with high voltage support and no dynamic load models, D) Transient Contingency with Dynamic DER Models with low voltage support and no dynamic load models, E) Transient Contingency with Dynamic Load Models and no dynamic DER models, F) Transient Contingency without Dynamic DER or Load Models, G) Steady State Contingency.

important to note that the current, load MW and Mvar, and DER MW and Mvar time-series output is not included in Figure 5.2 when no dynamic DER models are included. This is because when no dynamic DER models are included the DER contribution is taken directly out of the load and only the net load behavior exists as an output. In a transient contingency, a load without a dynamic load model exhibits constant impedance behavior. With a dynamic load model the load behavior includes induction motor components and other voltage dependent components. These differences result in a large active power and current dip in the load without dynamic loads and a large reactive power dip and current increase with dynamic load models. The active power dip without dynamic

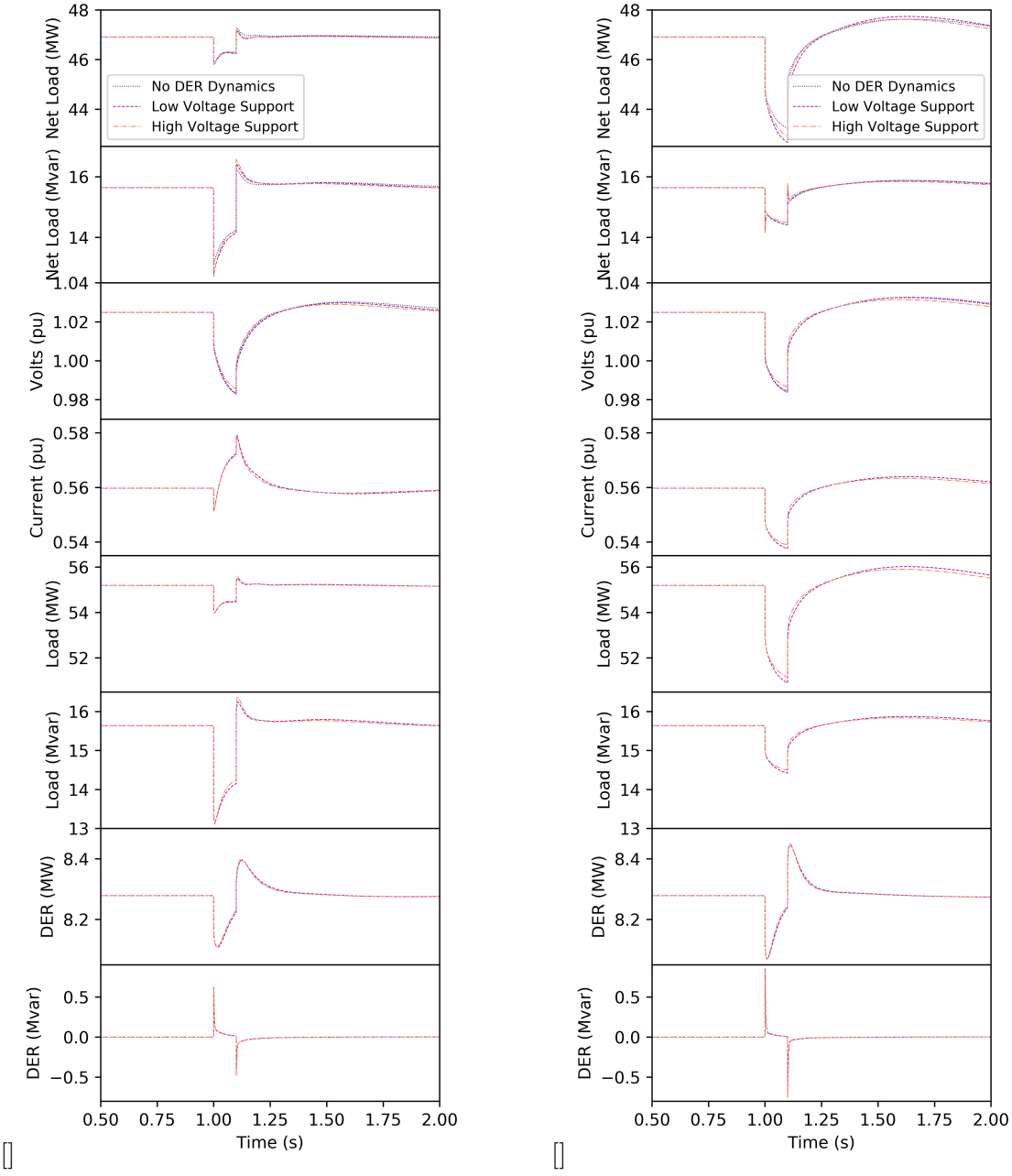

Figure 5.2: Time-series output from load bus 7051 for [a] scenarios with dynamic load models (A,B,E) and [b] scenarios without dynamic load models (C,D,F)

loads is representative of constant impedance behavior. The induction motor behavior with dynamic load models results in a high current draw and reactive power dip due to the deceleration of the induction motors [31]. The active power also has less swing when the dynamic loads are included due to less of the load having constant impedance behavior. Since the only additional behaviors that dynamic DER models bring are trip settings and voltage or frequency support controls, the dominant behavior between the two models is the dynamic load model. In both [a] and [b] one can see that the inclusion of voltage support reduces the voltage dip from the reactive power input provided by the DER. The reduction of this voltage dip between scenarios A and B explains the increase in HC. The reduction of the voltage dip between scenario C and D, without dynamic load models, does not increase the HC. It is possible that the voltage support plays less of a crucial role when dynamic load models are not present, and therefore does not have an impact on HC. When dynamic DER models are not included, as in the scenarios E and F, the DER contribution is taken directly from the load, so the net load behavior is based on the load model whether that be a static or voltage dependent model or a dynamic load model. Therefore when the dynamic DER model is not included what is missing is voltage support and the voltage dip is greater, which explains why in scenario F the HC is decreased.

The findings from this section demonstrate how the inclusion of voltage support controls on DERs can have a systemwide increase in HC, specifically when dynamic loads are considered in the system. It is important to note that dynamic loads are almost always present in real systems, the question is whether or not this behavior is represented in the models. There is around a 15% difference in HC between evaluations with steady state contingencies and transient contingencies. Whereas there is a maximum of a 5% difference between transient contingency scenarios. Though higher fidelity modeling included in transient contingencies provides greater insight into the provided system stability benefits due to DER controls and impacts from dynamic loads in the system, in general it is of greater importance to perform transient contingency evaluations over steady state contingencies as transient contingency conditions are more limiting and representative of the system's actual capabilities. If steady state contingencies or conditions are used to evaluate the HC of the system it is necessary for it to be understood that the reported HC is likely inflated or optimistic.

5.3 Dynamic Load Model Variation in Transmission HC

The experimental setup of this section is similar to Section 5.2, but with transient contingencies with both dynamic load and DER models. This section analyzes the parameters in the dynamic load models to evaluate how variability in the dynamic load behavior impacts HC. The parameters varied are the percentages of each type of load within the composite load model. These parameters were gathered with the Load Model Data Tool, with settings set to the shoulder season in the Texas regions, as the a Fall loading scenario is used for this section. The parameters were calculated for every hour of the day. An example of the parameters for one load at load bus 7051, which is set as a rural/agricultural feeder, are shown in Figure 5.3.

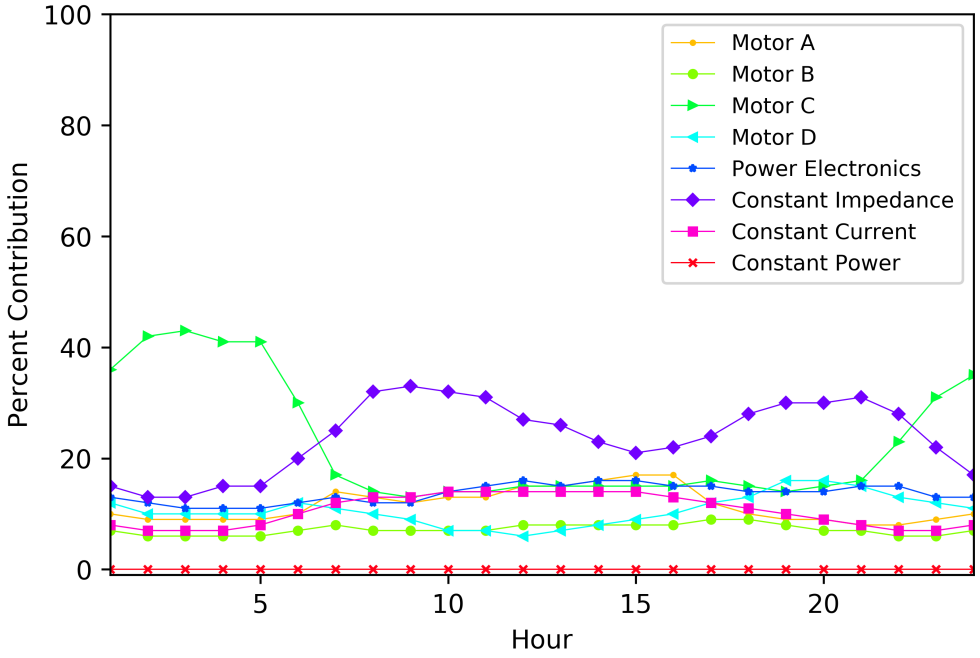

Figure 5.3: Hourly composite load model parameters for load bus 7051, a rural/agricultural load, during the shoulder season generated with the Load Model Data Tool Comparison.

The main shift in load behavior over the course of the day is between the constant impedance load and the motor c load which is representative of low inertia pump type motors.

5.3.1 Results

The variation in the load types throughout the day impacts the responses of the load. The impact of this shifting load profile on transient stability is demonstrated with the line fault on the line between buses 7304 and 7095 and shown in Figure 5.4. The figures show the time-series output from load 7051 with the hourly load parameters for (a) hours 1-12 and (b) hours 13-24.

One can see that as the load type shifts from majority motor based at hour 0 to majority constant impedance based at hour 12 the active power dip increases to represent more constant impedance behavior and the voltage recovery is a little higher. The HC was evaluated at each hour with the hourly load parameters and there was no change in HC. The change in dynamic load parameters are designed to be characteristic of the load types in Texas and this suggests that the variation in load behavior has a negligible impact on HC in this system. The variation in load behavior in other systems with different load profiles could impact the HC, especially in systems with diverse load behaviors or a high presence of induction motors which can negatively impact transient voltage stability. However, the finding for this system is that variation in dynamic load behavior is not critical for evaluating HC.

5.4 Impact of Seasonal and Loading Variations on Transmission HC

This section evaluates HC of the 2,000-bus synthetic system for different seasonal and loading scenarios. The seasonal and loading scenarios were developed in [95]. The evaluation of conditions, stability, and capability of systems throughout numerous seasons and loading is critical for operations and planning in transmission systems. For example, the Bonneville Power Administration incorporates seasonal base cases into their short-term available transfer capability (ATC) methodology [100]. The goal of the evaluation of HC across the seasonal and loading scenarios in this study is to highlight the impact that season and loading can have on HC and also to identify specific system conditions or factors that limit the HC.

The HC in this section was determined using $N-1$ line loss steady state contingencies. Steady state contingencies are used here instead of transient contingencies to reduce the computational burden of evaluating $N-1$ line loss contingencies, which total 3,206

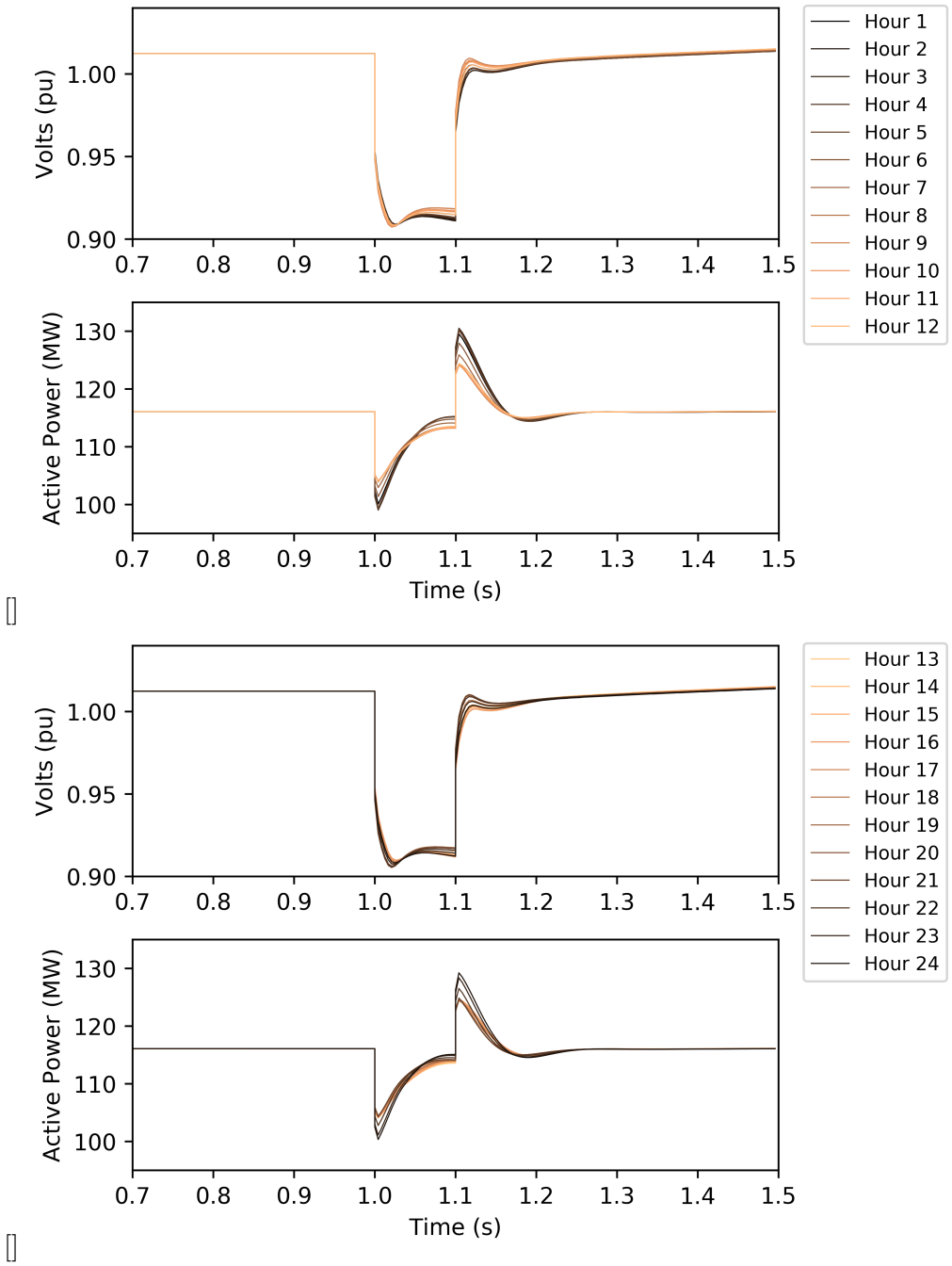

Figure 5.4: Time-series outputs from load 7051 with hourly composite load model parameters for [a] hours 1-12 and [b] hours 13-24

contingencies. The same number of allowed violations per contingency used in Section 5.2 are used to determine the HC in this section. In addition to the limits used in Section 5.2, 32 unsolved contingencies out of the 3,206 are also allowed before the limit of the HC is reached.

5.4.1 Results

A total of eight scenarios are evaluated in this section, a high (peak) and low loading for Spring, Summer, Fall, and Winter where each season has a different generation profile. These scenarios are generated from yearly time series data taken at the lowest and highest load time periods for each season. The resulting HC for each scenario is illustrated in Figure 5.5.

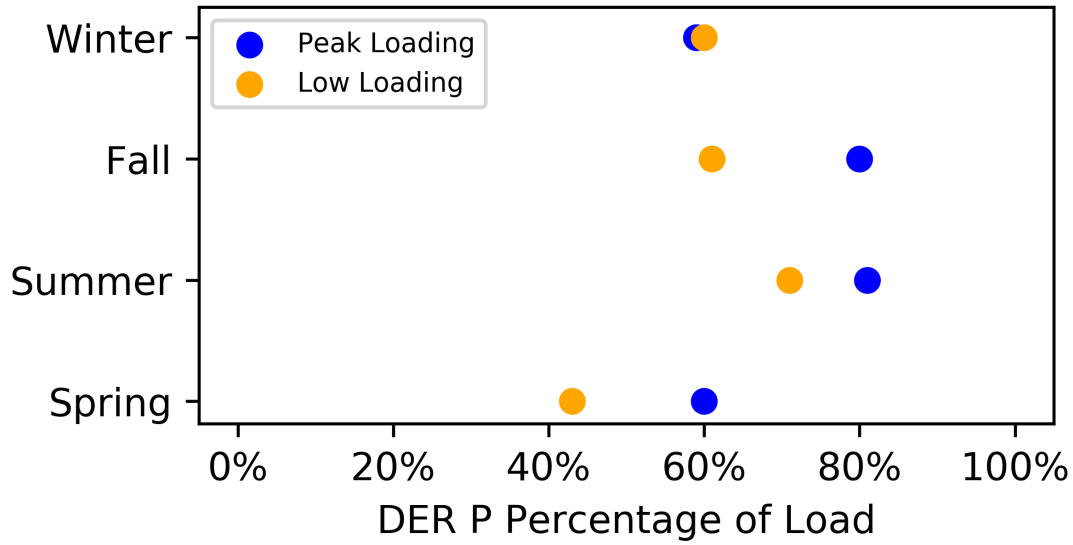

Figure 5.5: Seasonal hosting capacity results for high and low loading scenarios for each season. The high or peak loading is in blue and teh low loading is shown in orange.

The resulting HC across all seasons and loading scenarios varies greatly between seasons with a total range of 20%. Additionally, all but one season, winter, has high HC in the peak loading scenario in comparison to the low loading scenario. For explanation of these results the HC values were compared to several system level factors. The system

level factors included reserve amount, generation amount, and linear sensitivity factors such as weighted transmission loading relief (WTLR). The system level factors considered were:

1. Generation Amount (MW and Mvar)
2. Generation Downward Capability (MW and Mvar)
3. Generation Upward Capability (MW and Mvar)
4. Wind Generation (MW)
5. Generation Outage Capacity (MW)
6. Transmission Outage Capacity (MVA)
7. Percent of Branches over 50% loaded

The generation amount, downward and upward capability, generation outage capacity, and transmission outage capacity all relate and can act as a system reserve. Numerous studies have shown that system reserves impact the amount of wind generation that can be stably integrated in transmission systems [101], whose impact in terms of uncertainty and variability is similar to DERs. Since this test system has a high presence of wind generation both the wind generation and system reserves could be a limiting factor in HC. Additionally, in these test cases the dispatch of wind generation is not curtailed or determined by unit commitment. The percent of branches over 50% loaded is in reference to their pre-contingency state. Therefore, this percentage is likely impacted by wind generation amount, and could also be a potential limiting factor.

Each of these factors were compared against the HC for all scenarios to determine if trends arose to suggest if certain factors were key limiting or dominant factors. Of the factors evaluated, only three showed strong trends: reactive power generation amount, active power wind generation amount, and percent of branches over 50% loaded. These data and their corresponding trend-lines are shown in Figure C.1.

Since the trend between peak and low loading for each season was flipped for the winter season, the peak and low loading scenarios for the Fall and Winter months are annotated in Figure C.1. This is to show how the flip between peak and low loading also appears in the trend between the HC and system level factors.

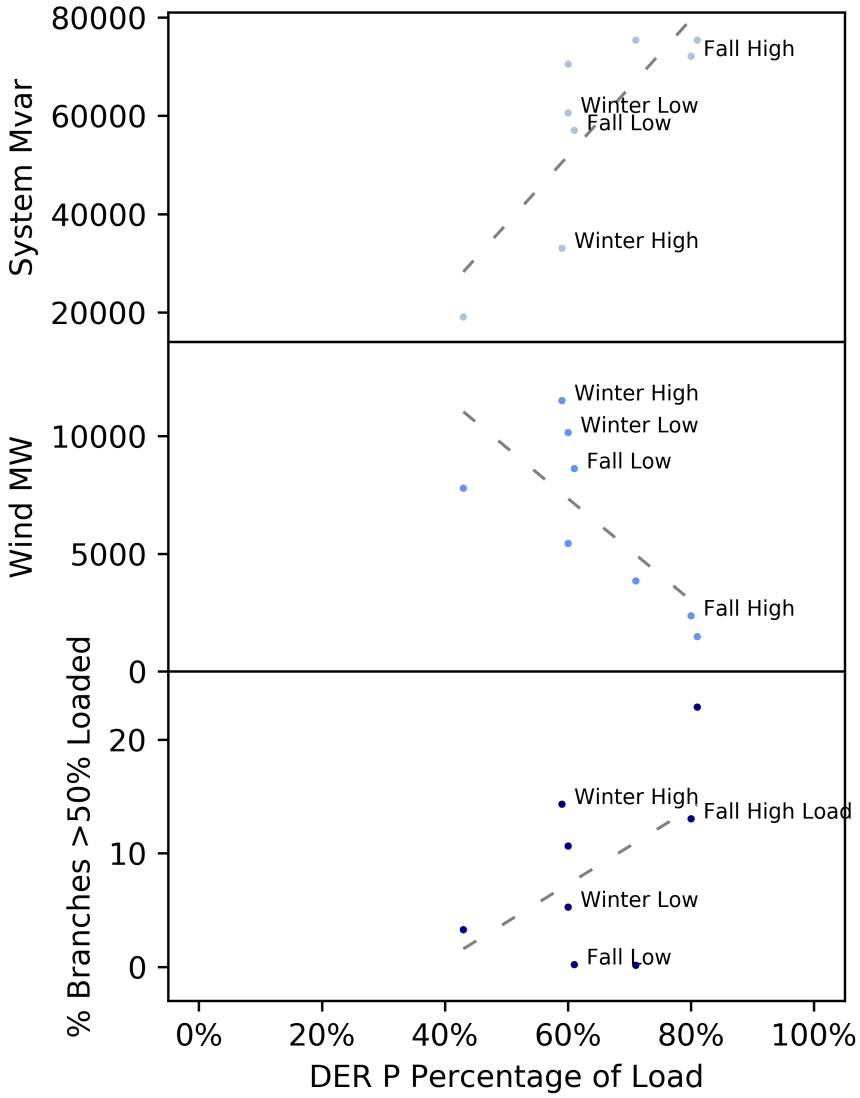

Figure 5.6: Trends between system conditions and hosting capacity

As the amount of reactive power in the system increases and the HC increases, this trend is seen throughout all scenarios. The amount of reactive power in the system contributes to the voltage stability. In distribution systems, increasing DER generation causes a reduction in voltage stability by causing over-voltage within a feeder. The

Table 5.2: R-values for correlation relationship between area location of limiting contingency elements and the violation elements of the contingency for against the amount of reactive power generation, active power wind generation, and percent of branches over 50% loaded in each area.

	Reactive Power Generation by Area	**Active Power Wind Generation by Area**	**Percent of Branches over 50% Loaded by Area**
Contingency Element Area	-0.014	0.511	0.480
Violation Element Area	0.106	0.604	0.396

trend seen here suggests that reactive power supply is also a limiting factor for HC in transmission systems as well. The increase in wind active power generation results in a decrease in HC. It is likely due to this shift in generation, specifically in the areas where wind generation is present, that causes greater stresses in the system as seen by the increase in percent of branches over 50% loaded that cause a decrease in HC. The effective reduction in load, due to an increase in DER contribution in these steady state contingencies, reduces the loading on the branches. Therefore, the greater the initial loading on branches present in the high loading seasonal scenarios the more room to accommodate DERs and greater the HC.

The HC trends were then compared to where the violations in the system occurred at the HC limit for each scenario. The contingency elements that caused more than 100 violation limits and the elements that reached a violation were binned into each of the areas of the system. The area locations of the contingency elements and the violation elements were then compared to the amount of reactive power generation, active power wind generation, and percent of branches over 50% loaded in each area. The test system has eight areas which combined with the eight seasonal and loading scenarios created 64 data points to compare to determine a correlation. The correlation r-values were calculated for these three factors and are shown in Table 5.2.

A strong correlation relationship exists with a r-value of 0.5 or greater for a strong positive relationship and -0.5 or lesser for a strong negative relationship. Strong relationships are seen between both contingency element area and violation element area and wind generation confirming the relationship between hosting capacity and wind gener-

ation. The greater the amount of wind generation the lower the hosting capacity. The relationship with branch loading is almost strong, and weak relationships exist with reactive power generation by area. It is also likely that the branch loading is a result from wind generation amount. We also note that the wind generation trend is the only one where the trend between high and low loading scenarios between Fall and Winter scenarios switches. There is greater wind generation during the winter high loading scenario than the winter low loading scenario. This flips for the Fall season where there is more wind generation in the Fall low loading scenario than the high loading scenario. This is the only factor where this flip in the trend between Winter and Fall low and high loading scenarios of hosting capacity and the system factor exists. This implies that the greatest determining factor in these scenarios is wind generation amount as it is the only factor whose trend applies to all high and low seasonal scenarios, including the flipped low and high loading scenarios in the Winter season. These results suggest that the most limiting factor toward HC of DERs in this test system is the amount of wind generation. In the setup of these scenarios wind generators do not participate in any curtailment or unit commitment and they are located in select areas, located in five out of the eight areas, versus throughout all areas of the system. This study also does not include DERs in unit commitment or dispatch or curtailment. This lack of dispatch control of wind generation and DERs from the utility reduces the stability of the system in the case of high penetration of DERs. Strategic curtailment of DERs and wind generation has the potential to increase the overall hosting capacity of DERs and is an area of future work. A key takeaway from these results is unit commitment and dispatch of all generation in the system plays an important role in the ability of the system to host DERs.

5.5 Conclusion

This paper outlines the increasing need to assess DER HC on the transmission grid as the generation contribution of DERs increases. This study investigates the impact of modeling factors on transmission HC results on the 2,000-bus synthetic grid overlaid on the Texas Interconnect. The modeling factors assessed include transient versus steady state contingencies, dynamic load and DER models including voltage support control, variation in dynamic load model composition, and seasonal and loading scenarios. The results demonstrate transient stability conditions are more limiting to HC than steady

state stability conditions. Within transient contingency evaluations of HC the results vary between only 5% of DER contribution versus near 20% between transient and steady state evaluations. The use of voltage support controls within the DER dynamic model are proven to increase the HC in the system by 4%. The dynamic load composition variation assessed for this system makes no impact on the HC, however it is not guaranteed to be insignificant for all transmission systems. The seasonal and loading variations illustrate great differences between the resulting HC and highlight the need to assess the HC for numerous system scenarios to confirm system capabilities, as is similarly done in utility operation and planning methods. The impact of wind generation in this system also becomes a critical factor to HC. This is likely due to dispatch strategy employed in this system and indicates the need for inclusion and evaluation of dispatch of all resources if DERs are going to be integrated in transmission systems at high contributions. Future work is aimed at addressing optimal placement of DERs in transmission systems for improved HC and also assessing HC of DERs in additional test systems. The assessment of the impact of uncertainty in all aspects of this study will also be addressed in future work.

Chapter 6: Conclusion

This work takes deep dives into planning procedures and methods aimed to improve the integration of renewable, decentralized, and variable resources into electrical grids ranging from minigrids to transmission systems. The goals of the integration of these resources is to transform electrical grids to meet climate and national security goals while maintaining affordability and reliability criteria.

The work in chapter two introduces and provides an open-source tool for minigrid planning for rural electrification. The tool consists of two parts: optimizing resource and equipment sizing to minimize cost per unit of energy, and distribution network design including reliability cost-benefit analysis. The tool demonstrates how when reliability is valued through loss of customer load the distribution network design shifts from radial to meshed, justifying the addition of redundant or looping lines. This work fills a critical gap in open-source minigrid or microgrid planning tools with the addition of the geographical distribution network design.

The results from the work in chapter three highlight the need for improved measurement-based dynamic load modeling techniques. The study found of the similarity measures and system response outputs tested that less than 20% of all simulated tests in this study resulted in statistically significant correlations. This raises awareness to the importance of careful selection and validation of similarity measures and response output metrics. Naive or untested selection of metrics can deliver inaccurate and misleading results.

Chapter four illustrates the interplay between dynamic loads and DERs on transient voltage stability in a system. The results identified that the addition of dynamic loads to the studied system containing DERs reduces the minimum voltage swings. However, taken from the opposite perspective the addition of DERs to the system containing dynamic loads improves the transient voltage stability of the system. If the hosting capacity of DERs were to be based off of transient voltage stability the hosting capacity will change based on the inclusion of dynamic loads in the system.

Finally, chapter five evaluates the impacts of different modeling strategies on the results of transmission hosting capacity of DERs. Traditionally hosting capacity of DERs

has been performed for distribution networks. This work shifts the assessment to transmission networks due to the increasing contribution DERs have made to transmission networks in the last decade. The results demonstrate transient stability conditions are more limiting to hosting capacity than steady state stability conditions and that voltage support controls within the DER dynamic model can increase the hosting capacity. In this test system the dynamic load composition variation made no impact on the hosting capacity. The seasonal and loading variations illustrate great differences between the resulting hosting capacity and highlight the need to assess the hosting capacity for numerous system scenarios to confirm system capabilities.

These works perform and evaluate methods which push the boundaries of traditional power system planning methods. They highlight current shortcoming and identify areas for growth. Power system planning methods would benefit from further development of dynamic modeling for both DERs and loads and consideration of reliability cost-benefit in rural electrification cases. Specifically, future investigations into computationally fast optimization methods of dynamic simulations could aid development of tools and guidelines used in power system planning to assist the sustainable, affordable, and reliable transformation of how we get our electricity.

Bibliography

[1] R. Thombs and A. Jorgenson, "The political economy of renewable portfolio standards in the united states," *Energy Research Social Science*, 04 2020.

[2] U. E. I. Administration, "Electric power sector energy consumption," 2 2020.

[3] T. Adefarati and R. Bansal, "Reliability, economic and environmental analysis of a microgrid system in the presence of renewable energy resources," *Applied Energy*, vol. 236, pp. 1089–1114, 2019.

[4] A. Lyden, R. Pepper, and P. Tuohy, "A modelling tool selection process for planning of community scale energy systems including storage and demand side management," *Sustainable Cities and Society*, pp. 674–688, 2018.

[5] G. Mendes, C. Ioakimidis, and P. Ferrão, "On the planning and analysis of integrated community energy systems: A review and survey of available tools," *Renewable and Sustainable Energy Reviews*, pp. 4836–4854, 2011.

[6] M. Gröissbock, "Are open source energy system optimization tools mature enough for serious use?," *Renewable and Sustainable Energy Reviews*, pp. 234–248, 2019.

[7] B. Bakken, H. Skjelbred, and O. Wolfgang, "etransport: Investment planning in energy supply systems with multiple energy carriers," *Energy*, vol. 32, pp. 1676–1689, 2007.

[8] M. Orosz and A. Mueller, "Dynamic simulation of performance and cost of hybrid pv-csp-lpg generator micro grids with applications to remote communities in developing countries," in *Proceedings of the Am. Soc. Mech. Eng. Power Energy Conf.*, 06 2015.

[9] "Reopt: A platform for energy system integration and optimization," tech. rep., National Renewable Energy Laboratory, 2017.

[10] L. B. N. Laboratory, *DER-CAM User Manual*. Department of ENergy.

[11] S. Sinha and S. Chandel, "Review of software tools for hybrid renewable energy systems," *Renewable and Sustainable Energy Reviews*, vol. 32, p. 192–205, 04 2014.

[12] S. Guo, *Improvements to Power System Dynamic Load Model Parameter Estimation*. PhD thesis, University of Illinois at Urbana-Champaign, 2017.

[13] "The history and evolution of the u.s. electricity industry," tech. rep., The University of Texas at Austin energy institute, July 2016.

[14] "Impact assessment of the 1977 new york city blackout," tech. rep., Systems Control, Inc., July 1978.

[15] "Goal 7: Affordable and clean energy," tech. rep., United Nations Development Programme, 2019.

[16] K. Balaraman, "PGE says power shutoffs averted hundreds of fire risks but cities blast lack of coordination," *Utility Dive*.

[17] "Energy access outlook 2017," tech. rep., International Energy Agency, 2017.

[18] "Lights, power, action: Electrifying africa," tech. rep., Africa Progress Panel, 2016.

[19] "Create your own microgrid control strategies with homer pro apis," tech. rep., HOMER Energy, 2016.

[20] B. G. V. M. L. A. Arribas, L and K. Mauch, "World-wide overview of design and simulation tools for hybrid pv systems," tech. rep., IEA, Jan 2011. Report IEA-PVPS T11-01:2011.

[21] "Renewables for sustainable village power," tech. rep., National Renewable Energy Laboratory, 2000.

[22] A. Chowdhury and D. Koval, "Current practices and customer value-based distribution system reliability planning," *IEEE Trans. Industry Applications*, vol. 40, pp. 1174–1182, 2004.

[23] M. Khodayar, M. Barati, and M. Shahidehpour, "Integration of high reliability distribution system in microgrid operation," *IEEE Trans. on Smart Grid*, vol. 3, pp. 1997–2006, 2012.

[24] S. Madathil, E. Yamangil, H. Nagarajan, A. Barnes, R. Bent, S. Backhaus, S. Mason, S. Mashayekh, and M. Stadler, "Resilient off-grid microgrids: Capacity planning and n-1 security," *IEEE Trans. on Smart Grid*, pp. 6511–6521, Nov. 2018.

[25] S. Chalil Madathil, H. Nagarajan, R. Bent, S. Mason, S. Eksioglu, and M. Lu, "Algorithms for optimal topology design, placement, sizing and operation of distributed energy resources in resilient off-grid microgrids," 06 2018.

[26] S. Sigarchian, M. Orosz, H. Hemond, and A. Malmquist, "Optimum design of a hybrid pv-csp-lpg microgrid with particle swarm optimization technique," *Applied Thermal Energy*, pp. 1031–1036, 2016.

[27] A. Malheiro, P. Castro, R. Lima, and A. Estanqueiro, "Integrated sizing and scheduling of wind/pv/diesel/battery isolated systems," *Renewable ENergy*, vol. 83, pp. 646–657, 2015.

[28] K. Wu, H. Zhou, S. An, and T. Huang, "Optimal coordinate operation control for wind-photovoltaic-battery storage power-generation units," *Energy Conversion and Management*, vol. 90, pp. 466–475, 2015.

[29] S. Singh, M. Singh, and S. Kaushik, "Feasibility study of an islanded microgrid in rural area consisting of pv, wind, biomass and battery energy storage system," *Energy Conversion and Management*, vol. 128, pp. 178–190, 2016.

[30] C. P. Generation, *Cummins Onan RV Generator Set Operator Manual*. Cummins Power Generation.

[31] Y. Xu, J. Ma, Z. Dong, and D. Hill, "Robust transient stability-constrained optimal power flow with uncertain dynamic loads," *IEEE Transactions on Smart Grid*, pp. 1991–1921, 2017.

[32] F. Pedregosa, G. Varoquaux, A. Gramfort, V. Michel, B. Thirion, O. Grisel, M. Blondel, P. Prettenhofer, R. Weiss, V. Dubourg, J. Vanderplas, A. Passos, D. Cournapeau, M. Brucher, M. Perrot, and E. Duchesnay, "Scikit-learn: Machine learning in Python," *Journal of Machine Learning Research*, vol. 12, pp. 2825–2830, 2011.

[33] P. Cicilio, M. Orosz, and A. Mueller, "uGrid: Minigrid Design and Planning Toolset." Zenodo, May 2019. https://doi.org/10.5281/zenodo.3236475.

[34] K. Shetye, T. Overbye, and T. Doern, "Assessment of discrepancies in load models across transient stability software packages," in *Proceedings of the 2015 IEEE Power & Energy Society General Meeting*, (Denver, CO, USA), pp. 1–5, IEEE, 2015.

[35] J.-K. Kim, K. An, J. Ma, J. Shin, K.-B. Song, J.-D. Park, J.-W. Park, and K. Hur, "Fast and reliable estimation of composite load model parameters using analytical similarity of parameter sensitivity," *IEEE Transactions on Power Systems*, pp. 663–671, 2016.

[36] E. Kontis, T. Papadopoulos, A. Chrysochos, and G. Papagiannis, "Measurement-based dynamic load modeling using the vector fitting technique," *IEEE Transaction on Power Systems*, pp. 338–351, 2016.

[37] Y. Zhang, A. Allen, and B.-M. Hodge, "Impact of distribution-connected large-scale wind turbines on transmission system stability during large disturbances," in *Proceedings of the 2014 IEEE PES General Meeting*, (National Harbor, MD, USA), IEEE, 2014.

[38] H. Renmu, M. Jin, and D. Hill, "Composite load modeling via measurement approach," *IEEE Trans. on Power Systems*, vol. 21, no. 2, pp. 1533–1553, 2006.

[39] B.-K. Choi, H.-D. Chiang, Y. Li, Y.-T. Chen, D.-H. Huang, and M. Lauby, "Measurement-based dynamic load models: derivation, comparison, and validation," *IEEE Transactions on Power Systems*, no. 3, pp. 1276 – 1283, 2006.

[40] J. Ma, R. He, Z.-Y. Dong, and D. Hill, "Measurement-based load modeling using genetic algorithms," in *Proceedings of the 2007 IEEE Congress on Evolutionary Computation*, (Singapore, Singapore), September 2007.

[41] B.-K. Choi and H.-D. Chiang, "Multiple solutions and plateau phenomenon in measurement-based load model development: Issues and suggestions," *IEEE Transactions on Power Systems*, no. 2, pp. 824–831, 2009.

[42] S. Son, S. Lee, D.-H. Choi, K.-B. Song, J.-D. Park, Y.-H. Kwon, K. Hur, and J.-W. Park, "Improvement of composite load modeling based on parameter sensitivity and dependency analyses," *IEEE Transaction on Power Systems*, pp. 242–250, 2014.

[43] J. Ma, D. Han, R.-M. He, Z.-Y. Dong, and D. Hill, "Reducing identified parameters of measurement-based composite load model," *IEEE Transaction on Power Systems*, pp. 76–83, 2008.

[44] D. Kosterev, A. Meklin, J. Undrill, B. Lesieutre, W. Price, D. Chassin, R. Bravo, and S. Yang, "Load modeling in power system studies: Wecc progress update," in *Proceedings of the 2008 IEEE Power and Energy Society General Meeting - Conversion and Delivery of Electrical Energy in the 21st Century*, (Pittsburgh, PA, USA), pp. 1–8, IEEE, 2008.

[45] I. Visconti, D. Lima, J. de Sousa Costa, and N. de B.C. Sobrinho, "Measurement-based load modeling using transfer functions for dynamic simulations," *IEEE Transactions on Power Systems*, no. 1, pp. 111–120, 2014.

[46] Y. Kong and S. Liu, "Power system transient stability assessment based on geometric features of disturbed trajectory and dtw," in *Proceedings of the Sixth International Conference on Natural Computation*, (Yantai, China), pp. 485–489, August 2010.

[47] C. Grigg, P. Wong, P. Albrecht, R. Allen, M. Bhavaraju, R. Billinton, Q. Chen, C. Fong, S. Haddad, S. Kuruganty, W. Li, R. Mukerji, D. Patton, N. Rau, D. Reppen, A. Schneider, M. Shahidehpour, and C. Singh, "The IEEE reliability test system-1996. a report prepared by the reliability test system task force of the application of probability methods subcommittee," *IEEE Trans. Power Syst*, no. 3, pp. 1010–1020, 1999.

[48] C. Lassetter, E. Cotilla-Sanchez, and K. Jinsub, "Enhanced ieee rts-96 test case w/synthesized dynamic parameters [dataset]." Zenodo, 2016. https://zenodo.org/record/51001#.WxoDk0gvxPZ.

[49] C. Marcy, J. Logan, J. McCall, F. Flores-Espino, A. Bloom, J. Aabakken, W. Cole, T. Jenkins, G. Porro, and C. Liu, "Electricity generation baseline report," tech. rep., National Renewable Energy Laboratory, 2016.

[50] S. Muhanji, A. Muzhikyan, and A. Farid, "Distributed control for distributed energy resources: Long-term challenges and lessons learned," *IEEE Access*, pp. 32737–32753, 07 2018.

[51] "Distributed energy resources: Technical considerations for the bulk power system," tech. rep., Federal Energy Regulatory Commission.

[52] A. M. Azmy and I. Erlich, "Impact of distributed generation on the stability of electrical power system," in *IEEE Power Engineering Society General Meeting, 2005*, pp. 1056–1063 Vol. 2, June 2005.

[53] J. Le Baut, P. Zehetbauer, S. Kadam, B. Bletterie, N. Hatziargyriou, J. Smith, and M. Rylander, "Probabilistic evaluation of the hosting capacity in distribution networks," in *2016 IEEE PES Innovative Smart Grid Technologies Conference Europe (ISGT-Europe)*, pp. 1–6, Oct 2016.

[54] M. Reza, P. Schavemaker, J. Slootweg, W. Kling, and L. van der Sluis, "Impacts of distributed generation penetration levels on power systems transient stability," in *Proceedings of the 2004 Power Engineering Society General Meeting*, (Denver, CO, USA), IEEE, 2004.

[55] V. N. Arava and L. Vanfretti, "A method to estimate power system voltage stability margins using time-series from dynamic simulations with sequential load perturbations," *IEEE Access*, pp. 43622–43632, 08 2018.

[56] C. Schwaegerl, M. Bollen, K. Karoui, and A. Yagmur, "Voltage control in distributed systems as a limitation of the hosting capacity for distributed energy resources," *18th International Conference and Exhibition on Electricity Distribution*, 06 2005.

[57] Z. Cheng and X. Feng, "A study of der volt and var droop aggregation for reactive power support to transmission system," in *2018 IEEE Power Energy Society General Meeting (PESGM)*, pp. 1–5, Aug 2018.

[58] B. A. Robbins, A. D. Domínguez-García, and C. N. Hadjicostis, "Control of distributed energy resources for reactive power support," in *2011 North American Power Symposium*, pp. 1–5, Aug 2011.

[59] Z. Wu, W. Gai, T. Gao, W. Yan, H. Zhang, S. Yan, and X. Wang, "State-of-the-art review on frequency response of wind power plants in power systems," *Journal of Modern Power Systems and Clean Energy*, pp. 1–16, 2018.

[60] R. Eriksson, N. Modig, and K. Elkington, "Synthetic inertia versus fast frequency response: a definition," *IET Renewable Power Generation*, pp. 507–514, year=2018, publisher=IET.

[61] S. Datta and V. Vittal, "Operational risk metric for dynamic security assessment of renewable generation," *IEEE Transactions on Power Systems*, pp. 1389–1399, 03 2017.

[62] S. Datta and V. Vittal, "A diagnostics tool for risk-based dynamic security assessment of renewable generation," in *2018 IEEE International Conference on Probabilistic Methods Applied to Power Systems (PMAPS)*, pp. 1–6, June 2018.

[63] F. Tuffner, K. Schneider, J. Hansen, and M. Elizondo, "Modeling load dynamics to support resiliency-based operations in low-inertia microgrids," *IEEE Transactions on Smart Grid*, 05 2019.

[64] A. P. S. Meliopoulos, G. Cokkinides, and G. Stefopoulos, "Voltage stability and voltage recovery: load dynamics and dynamic var sources," in *2006 IEEE Power Engineering Society General Meeting*, pp. 8 pp.–, June 2006.

[65] M. A. Mahmud, M. J. Hossain, and H. R. Pota, "Effects of large dynamic loads on power system stability," *International Journal of Electrical Power & Energy Systems*, pp. 357–363, 2013.

[66] S. Abdelaziz, B. Khadija, and E. Mohamed, "Assessment of wind power penetration level in distribution network with consideration of static, motor and composite loads," *2014 5th International Renewable Energy Congress*, 03 2014.

[67] "900 MW fault induced solar photovoltaic resource interruption disturbance report," tech. rep., North American Electric Reliability Corporation, 2017.

[68] California Public Utilities Commission, "Rule 21 interconnection," 2017. Available: `https://www.cpuc.ca.gov/Rule21/`.

[69] "WECC dynamic composite load model (CMPLDW) specifications." Online, Jan. 27, 2015.

[70] P. Cicilio and E. Cotilla-Sanchez, "Evaluating measurement-based dynamic load modeling techniques and metrics," *IEEE Transactions on Power Systems*, pp. 1–1, 2019.

[71] P. E. David Chassin, "Load model data tool, version 00," 4 2013.

[72] J. P. Lopes, N. Hatziargyriou, J. Mutale, P. Djapic, and N. Jenkins, "Integrating distributed generation into electric power systems: a review of drivers, challenges and opportunities," *Electric Power Systems Research*, pp. 1189–1203, 2007.

[73] G. Pepermans, J. Driesen, D. Haeseldonckx, R. Belmans, and W. D'haeseleer, "Distributed generation: definition, benefits and issues," *Energy Policy*, pp. 787–798, 2005.

[74] A. Keane, L. Ochoa, C. L. Borges, G. Ault, A. Alarcon-Rodriguez, R. Currie, F. Pilo, C. Dent, and G. Harrison, "State-of-the-art techniques and challenges ahead for distributed generation planning and optimization," *IEEE Transactions on Power Systems*, pp. 1493–1502, 2012.

[75] M. Akorede, H. Hizam, and E. Pouresmaeil, "Distributed energy resources and benefits to the environment," *Renewable and Sustainable Energy Reviews*, pp. 724–734, 2010.

[76] S. Ismael, S. H. A. Aleem, A. Y. Abdelaziz, and A. F. Zobaa, "State-of-the-art of hosting capacity in modern systems with distributed generation," *Renewable Energy*, pp. 1002–1020, 2019.

[77] H. Al-Saadi, R. Zivanovic, and S. Al-Sarawi, "Probabilistic hosting capacity for active distribution networks," *IEEE Transaction on Industrial Informatics*, pp. 2519–2532, 2017.

[78] M. Zangiabadi, R. Feuillet, H. Lesani, N. Hadj-Said, and J. Kvaløy, "Assessing the performance and benefits of customer distributed generation developers under uncertainties," *IEEE Transactions on Sustainable Energy*, pp. 1935–1947, 2018.

[79] M. Abad, J. Ma, D. Zhang, A. Ahmadyar, and H. Marzooghi, "Probabilistic assessment of hosting capacity in radial distribution systems," *IEEE Transactions on Sustainable Energy*, pp. 1935–1947, 2018.

[80] S. M. Mirbagheri, D. Falabretti, V. Ilea, and M. Merlo, "Hosting capacity analysis: A review and a new evaluation method in case of parameters uncertainty and multi-generator," in *Proceedings of the 2018 EEEIC / ICPS Europe*, (Palermo, Italy), pp. 1–6, IEEE, 2018.

[81] Federal Energy Regulatory Commission, "Electric storage participation in markets operated by regional transmission organizations and independent system operators," tech. rep., February 2018.

[82] P. Raja, M. Selvan, and N. Kumaresan, "Enhancement of voltage stability margin in radial distribution system with squirrel cage induction generator based distributed generators," *IET Generation, Transmission Distribution*, pp. 898–906, 2013.

[83] P. Divshali and L. Söder, "Improving pv hosting capacity of distributed grids considering dynamic voltage characteristic," in *Proceedings of the 2018 PSCC*, (Dublin, Ireland), IEEE, 2018.

[84] C. Yammani, G. Maheswarapu, and S. Matam, "Optimal placement and sizing of der's with load models using a modified teaching learning based optimization algorithm," in *Proceedings of the 2014 ICGCCEE*, (Coimbatore, India), IEEE, 2014.

[85] A. El-Zonkoly, "Optimal placement of multi-distributed generation units including different load models using particle swarm optimisation," *IET Generation, Transmission Distribution*, pp. 760–771, 2011.

[86] D. Hung, N. Mithulananthan, and K. Lee, "Determining pv penetration for distribution systems with time-varying load models," *IEEE Transactions on Power Systems*, pp. 3048–3057, 2014.

[87] T. de Oliveira, M. Bollen, P. Ribeiro, P. de Carvalho, A. Zambroni, and B. Bonatto, "The concept of dynamic hosting capacity for distributed energy resources: Analytics and practical considerations," *energies*, 2019.

[88] C. Rathore and R. Roy, "Impact of distributed generation in transmission network expansion planning problem," in *Proceedings of the 2013 3rd International Conference on Electric Power and Energy Conversion Systems*, (Istanbul, Turkey), IEEE, 2013.

[89] P. Gomes and J. Saraiva, "Transmission system planning considering solar distributed generation penetration," in *Proceedings of the 2017 14th International Conference on the European Energy Market*, (Dresen, Germany), IEEE, 2017.

[90] N. Matute, S. Torres, and C. Castro, "Transmission expansion planning considering the impact of distributed generation," in *Proceedings of the 2019 IEEE PES ISGT-Europe*, (Bucharest, Romania), IEEE, 2019.

[91] J. Zhao, J. Foster, Z. Dong, and K. Wong, "Flexible transmission network planning considering distributed generation impacts," *IEEE Transactions on Power Systems*, pp. 1434–1443, 2011.

[92] J. Qiu, Z. Dong, J. Zhao, Y. Xu, F. Luo, and J. Yang, "A risk-based approach to multi-stage probabilistic transmission network planning," *IEEE Transactions on Power Systems*, pp. 4867–4876, 2016.

[93] P. Pena, N. Morales, M. Artenstein, A. Pizzini, and C. Zoppolo, "Planning in transmission systems with a great level of penetration of distributed generation," in *Proceedings of the 2015 Innovative Smart Grid Technologies Latin America*, (Montevideo, Uruguay), pp. 87–91, IEEE, 2015.

[94] J. Wang, H. Zhong, Q. Xia, and C. Kang, "Optimal planning strategy for distributed energy resources considering structural transmission cost allocation," *IEEE Transactions on Smart Grid*, pp. 5236–5248, 2018.

[95] H. Li, J. Yeo, J. Wert, and T. Overbye, "Steady-state scenario development for synthetic transmission systems," in *Proceedings of the 2020 Texas Power and Energy Conference*, (College Station, Texas), IEEE, 2020.

[96] A. Kumar and S. Sirvastva, "AC power transfer distribution factors for allocating power transactions in a deregulated market," *IEEE Power Engineering Review*, July 2002.

[97] J. Milanovic, K. Yamashita, S. Villanueva, S. Djokic, and L. Korunovic, "International industry practice on power system load modeling," *IEEE Transaction on Power Systems*, pp. 3038–3046, 2013.

[98] D. Han, J. Ma, R. He, and Z.-Y. Dong, "A real application of measurement-based load modeling in large-scale power grids and its validation," *IEEE Transactions on Power Systems*, pp. 1756–1764, 2009.

[99] PowerWorld Corporation, "Model DER_A distributed energy resource aggregate model," tech. rep., 2020.

[100] Bonneville Power Authority, "Automation, improved modeling may lead to more transmission sale," 1 2020.

[101] M. Milligan, P. Donohoo, D. Lew, E. Ela, B. Kirby, H. Holttinen, E. Lannoye, D. Flynn, M. O'Malley, N. Miller, P. Eriksen, A. Gøttig, B. Rawn, J. Frunt, W. Kling, M. Gibescu, E. Làzaro, A. Robitaille, and I. Kamwa, "Operating reserves and wind power integration: An international comparison," tech. rep., October 2010.

APPENDICES

Appendix A: All Published Works

Phylicia Cicilio, Eduardo Cotilla-Sanchez, Jake Gentle, "Transient Voltage Stability Effects on Hosting Capacity of Behind-the-Meter Devices", 2020 IEEE Power and Energy Society General Meeting.

Phylicia Cicilio, Lisa Swartz, Bjorn Vaagensmith, Tim McJunkin, Craig Rieger, Jake Gentle, and Eduardo Cotilla-Sanchez, "Electrical Grid Resilience Metric with Uncertainty", Power Systems Computation Conference 2020.

Phylicia Cicilio, Matthew Orosz, Amy Mueller, and Eduardo Cotilla-Sanchez, "uGrid: Reliable Minigrid Design and Planning Toolset for Rural Electrification", IEEE Access, 2019.

Phylicia Cicilio and Eduardo Cotilla-Sanchez, "Evaluating Measurement-Based Dynamic Load Modeling Techniques and Metrics", IEEE Transactions on Power Systems, 2019.

Phylicia Cicilio and Eduardo Cotilla-Sanchez, "Dynamic Composite Load Model Priority Placement Based on Electrical Centrality", 2018 IEEE Power and Energy Society General Meeting, 2018.

Kelly Tray, Phylicia Cicilio, Ted Brekken and Eduardo Cotilla-Sanchez, "Dynamic Composite Load Signature Detection and Classification using Supervised Learning over Disturbance Data", 2017 IEEE Energy Conversion Congress and Exposition, 2017

Appendix B: Twelve Bus System

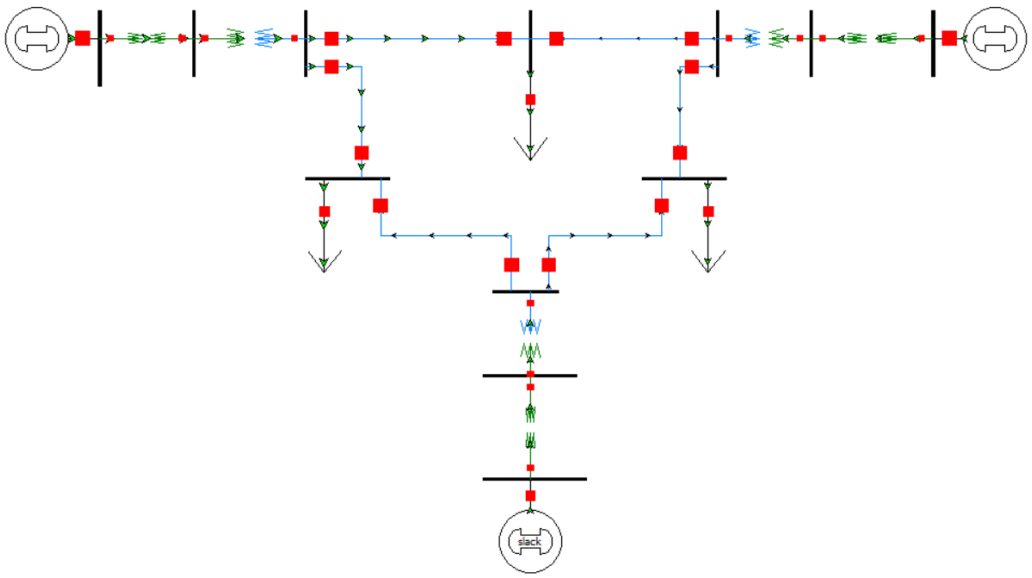

Figure B.1: Twelve bus test system used in chapter 4

Appendix C: 2000 Bus Synthetic Grid System

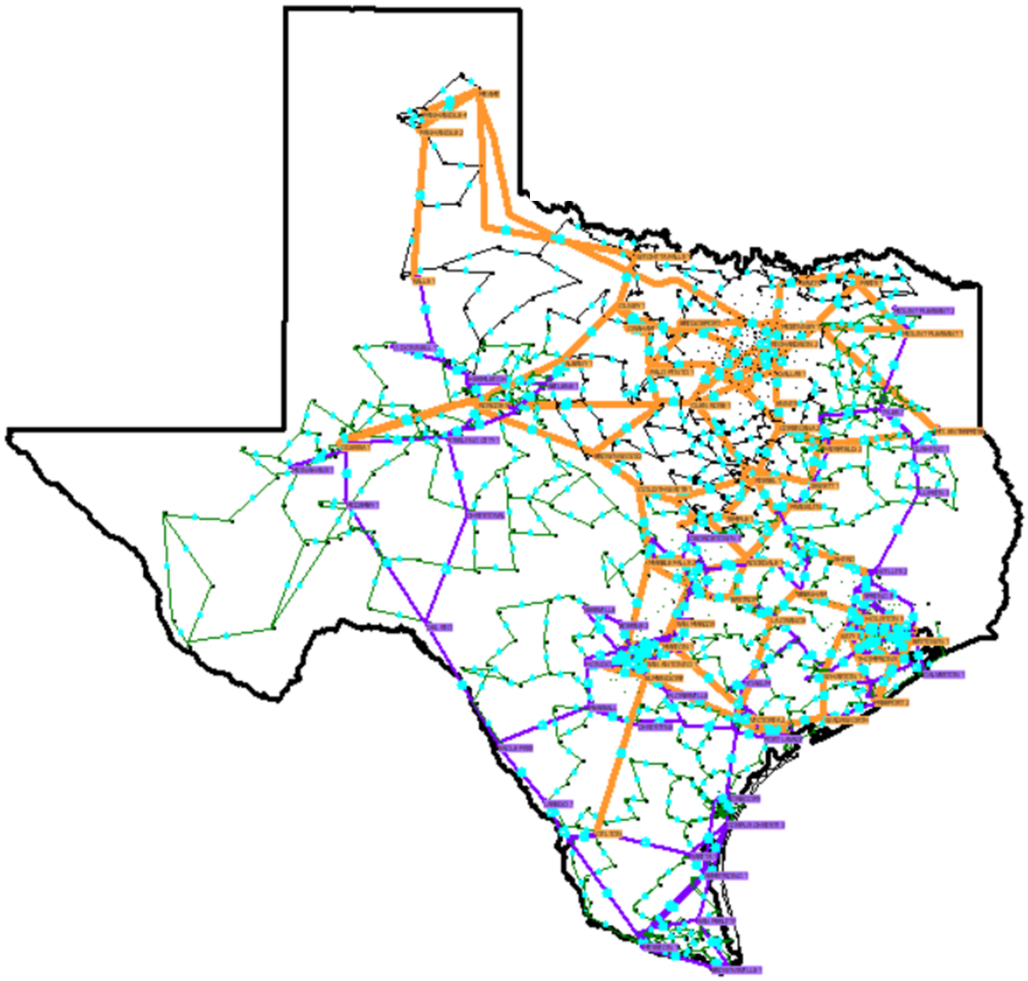

Figure C.1: 2000 bus synthetic grid system overlaid on the geographical footprint of Texas used in chapter 5.